IEEE Access
Multidisciplinary | Rapid Review | Open Access Journal

Received November 11, 2019, accepted November 27, 2019, date of publication December 4, 2019,
date of current version December 18, 2019.

Digital Object Identifier 10.1109/ACCESS.2019.2957544

Vector Control-Based Singularity Avoidance/Escape Steering Law for Single Gimbal Control Moment Gyros

NING MAO[1,2,3], TAO ZHANG[1,2], KAI XU[1,2,3], MAO-SHENG CHEN[1,2,3], AND CHAO DONG[1,2]

[1]Changchun Institute of Optics, Fine Mechanics and Physics, Chinese Academy of Sciences, Changchun 130033, China
[2]University of Chinese Academy of Sciences, Beijing 100190, China
[3]Chang Guang Satellite Technology Company, Ltd., Changchun 130000, China

Corresponding author: Mao-Sheng Chen (chenms_cgst@163.com)

This work was supported in part by the China Science and Technology Association Youth Talent Lifting Project under Grant 2017QNRC001, and in part by the Important Key Technologies R& D Program of Jilin under Grant 20170204069GX.

ABSTRACT The single-gimbal control moment gyros (SGCMGs) steering law has been a standing topic in the field of spacecraft attitude control for several decades. A practical steering law should meet the following requirements simultaneously: powerful singularity avoidance ability, high precision torque output ability and fast singularity escape ability. Moreover, the angular velocity commands generated by the steering law should not jitter sharply. In this paper, a vector control-based singularity avoidance and escape steering law for SGCMGs is proposed to satisfy these goals. In addition, a system angular momentum state evaluation function for command torque is defined for the first time, which can be used to effectively evaluate the remaining angular momentum resources for the command torque. We demonstrate the effectiveness and superiority of the proposed steering law with detailed comparisons to existing efforts.

INDEX TERMS Steering law, SGCMG, satellite attitude control.

I. INTRODUCTION

As a spacecraft attitude control unit, single gimbal control moment gyro (SGCMG) has significant torque magnification capability. It is of great importance to engineering application on large spacecraft and small smart satellites. However, there are geometric singularity problems inherent in the system with single gimbal control moment gyros (SGCMGs). When the output torque direction of all SGCMG is in the same plane or even the same line, the SGCMGs system will not have the torque output capacity of the three axes in the space, so that the spacecraft will lose the control ability of the three-axis attitude which is called the singular state. In order to avoid singularity, the SGCMGs usually adopt redundancy design. The minimum system is usually composed by four SGCMGs. Under redundant design, the singularity analysis and the steering algorithm of SGCMGs have become the focus of research in this field [1]–[31].

The existing steering laws can be roughly classified into three categories: singularity avoidance steering law, singularity escape steering law, and hybrid steering law. The hybrid steering law is designed based on the first two methods [22].

The main purpose of the singularity avoidance steering laws is to prevent the system from encountering the singular state. Most of these methods avoid the singular state of the system by adding appropriate null motion in advance, while a few avoid singularity by introducing torque error. The typical singularity avoidance steering laws include local gradient method (LG) [4], [22], non-directional null-motion algorithm (ND) [4], preferred gimbal angles method [7], and global avoidance methods [3], [6], [8]–[10]. They can be further divided into two categories: real-time singularity avoidance steering law and non-real-time singularity avoidance steering law. The real-time singularity avoidance algorithms are relatively small in computation, but they cannot evade all the

The associate editor coordinating the review of this manuscript and approving it for publication was Baoping Cai.

singular gimbal angles. Moreover, these algorithms often fail to make the system escape from the singularity quickly when the system falls into an inescapable internal singularity. The non-real-time singularity avoidance steering laws can avoid all the singularities. However, they cannot be applied to real-time tasks.

The main purpose of the singularity escape steering laws is to make the system escape from the singular state quickly. The typical singularity escape steering laws include singularity robust steering law (SR) [11], generalized singularity robust inverse method (GSR) [11], singular direction avoidance steering law (SDA) [13]–[15], and singularity escape steering laws based on singular surface [16]–[19]. Since these methods cannot avoid the singularity, they mainly rely on the torque error to make the system escape from singularity. However, the use of the torque error will reduce the overall performance of SGCMGs system.

The hybrid steering algorithm combines the advantages of the above two steering methods. It avoids the singularity through the null-motion or torque error. When the above process fails, it adopts the singularity escape strategy [12], [20]–[23]. Therefore, the hybrid steering law is more applicable to the engineering applications [25].

Despite decades of research, the steering law still has room for improvement. The ideal steering law should have strong singularity avoidance ability, high precision of moment output, fast singularity escape ability, and stable angular velocity command. However, most of the existing steering laws cannot possess these properties simultaneously.

To meet the above requirements simultaneously, a new hybrid steering method named vector-control based singularity avoidance and escape steering law (VCBSAE) is proposed in this paper. The proposed method defines the effective residual angular momentum evaluation function of each SGCMG for the desired torque. Based on this evaluation function, we design a set of desired gimbal angular velocity that can avoid singularity effectively. In the singularity avoidance process, the angular velocity command given by the steering law is approximated to the desired angular velocity by adding appropriate null motion in real time. If the singularity avoidance algorithm fails or the system is started at a singular state, the proposed steering law will switch to the singularity escape process automatically and smoothly. In this process, the algorithm will introduce a torque error and directly integrate the desired angular velocity into the command angular velocity, so that the system can quickly escape from singularity. In addition, a function used to evaluate the angular momentum state of the system for the command torque is defined. It can be used to judge whether the angular momentum resources of the system are sufficient for the command torque. If the system angular momentum reserve is sufficient, it is valuable to carry out singularity escape control when the system encounters the singularity. Otherwise the system angular momentum desaturation manipulation should be considered. If the angular momentum reserve of the system has been exhausted, desaturation manipulation should also be enabled. The effectiveness and superiority of the proposed algorithm are verified by comparing it with pseudo-inverse (PI) steering law, ND steering law [4], GSR steering law [11], ODSR steering law [12] and DSEA steering law [23].

The paper is organized as follows. Section II gives the system model of SGCMGs. Section III analyses the steering laws of ND, GSR, ODSR and DSEA. In section IV, we define the desired angular velocity of SGCMGs and explain the proposed VCBSAE steering law in details. Experimental results are provided in Section V. We then briefly conclude on the method and the performance in Section VI.

II. MODELING SYSTEMS WITH SGCMGs

A. SYSTEM MODEL

The schematic diagram of the SGCMG is shown in Fig. 1. It consists a gimbal motor and a spinning rotor. The characters τ_{in}, $\dot{\delta}_g$, and $\mathbf{g}$ denote the input torque, rotation speed, and gimbal axis of the gimbal motor, respectively. The characters $\mathbf{w}_r$ and $\mathbf{h}_r$ denote the angular speed and angular momentum of the spinning rotor, respectively. $\mathbf{O}$ is the output torque of the SGCMG, $\mathbf{W}_b$ is the rotation speed of the SGCMG under the action of $\mathbf{O}$.

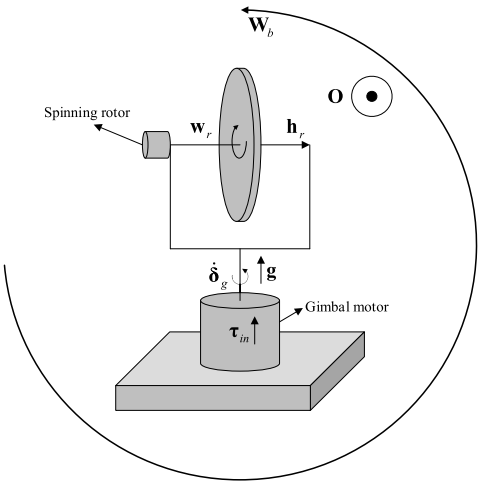

FIGURE 1. Schematic diagram of SGCMG.

For the design of the steering law, we only focus on the relationship between $\mathbf{O}$ and $\dot{\delta}_g$, as expressed in (1).

$$\mathbf{O} = \lim_{\Delta t\to 0} -\frac{\Delta \hat{\mathbf{h}}_r}{\Delta t} = \lim_{\Delta t\to 0} -\frac{\Delta t\dot{\delta}_g \times \hat{\mathbf{h}}_r}{\Delta t} = -\dot{\delta}_g \times \hat{\mathbf{h}}_r \quad (1)$$

$$\begin{aligned}
\boldsymbol{\tau}_{out} &= \mathbf{o}_1 + \mathbf{o}_2 + \mathbf{o}_3 + \mathbf{o}_4 \\
&= -\left(\dot{\boldsymbol{\delta}}_1 \times \mathbf{h}_1 + \dot{\boldsymbol{\delta}}_2 \times \mathbf{h}_2 + \dot{\boldsymbol{\delta}}_3 \times \mathbf{h}_3 + \dot{\boldsymbol{\delta}}_4 \times \mathbf{h}_4\right) \\
&= -(\hat{\mathbf{o}}_1(\hat{\dot{\boldsymbol{\delta}}}_1 \cdot \hat{\mathbf{g}}_1)\dot{\delta}_1 h_1 + \hat{\mathbf{o}}_2(\hat{\dot{\boldsymbol{\delta}}}_2 \cdot \hat{\mathbf{g}}_2)\dot{\delta}_2 h_2 \\
&\quad + \hat{\mathbf{o}}_3(\hat{\dot{\boldsymbol{\delta}}}_3 \cdot \hat{\mathbf{g}}_3)\dot{\delta}_3 h_3 + \hat{\mathbf{o}}_4(\hat{\dot{\boldsymbol{\delta}}}_4 \cdot \hat{\mathbf{g}}_4)\dot{\delta}_4 h_4) \\
&= h_0 \begin{bmatrix} -\hat{\mathbf{o}}_1 & -\hat{\mathbf{o}}_2 & -\hat{\mathbf{o}}_3 & -\hat{\mathbf{o}}_4 \end{bmatrix} \begin{bmatrix} (\hat{\dot{\boldsymbol{\delta}}}_1 \cdot \hat{\mathbf{g}}_1)\dot{\delta}_1 \\ (\hat{\dot{\boldsymbol{\delta}}}_2 \cdot \hat{\mathbf{g}}_2)\dot{\delta}_2 \\ (\hat{\dot{\boldsymbol{\delta}}}_3 \cdot \hat{\mathbf{g}}_3)\dot{\delta}_3 \\ (\hat{\dot{\boldsymbol{\delta}}}_4 \cdot \hat{\mathbf{g}}_4)\dot{\delta}_4 \end{bmatrix} \\
&= h_0 \mathbf{J}\dot{\boldsymbol{\delta}} \qquad (2)
\end{aligned}$$

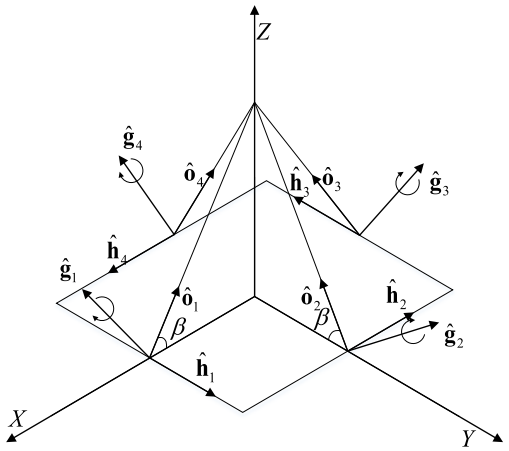

FIGURE 2. Pyramid configuration SGCMGs.

Fig. 2 shows a pyramid-configured SGCMGs. Many documents have chosen this configuration, which is convenient for the subsequent experiments. Compared with other configurations such as roofs, pyramid configuration contains all kinds of singularity types, which can test the performance of the proposed steering law better.

In this paper, for a vector $\mathbf{h}$, its unit vector and modulus are represented by $\hat{\mathbf{h}}$ and h, respectively. The characters $\hat{\mathbf{g}}_i$, $\hat{\mathbf{h}}_i$, $\hat{\mathbf{o}}_i$, and δ_i denote the unit vector of the gimbal axis, unit vector of rotor momentum, unit vector of output torque, and gimbal angles of a SGCMG where i=1,2,3,4. The skew angle of the pyramid is denoted by β. In Fig. 2, the system is in the initial position, $\delta_1 = \delta_2 = \delta_3 = \delta_4 = 0°$. We define the counter-clockwise rotation direction of the gimbal motor as the positive direction, and the rotation direction shown in Fig. 2 is clockwise. According to Fig. 2, the total output moment of pyramid SGCMGs is expressed as (2). Note that $h_1 = h_2 = h_3 = h_4 = h_0$, and $\mathbf{J}$ is the Jacobian matrix.

B. SINGULARITY PROBLEM

Refer to Fig. 2, $\hat{\mathbf{o}}_i$ are defined in three-dimensional space, it is a function of δ_i and can span a three-dimension space at most. Equation (2) shows that the output torque $\boldsymbol{\tau}_{out}$ of the SGCMGs is located in the space spanned by $\hat{\mathbf{o}}_i$, and $\hat{\mathbf{o}}_i$ is the column of $\mathbf{J}$. Therefore, the rank of $\mathbf{J}$ can be used to determine whether the system is in a singular state. If rank($\mathbf{J}$) = 3, $\boldsymbol{\tau}_{out}$ can be any vector in the three-dimension space, and the system is nonsingular. Otherwise, $\boldsymbol{\tau}_{out}$ is limited to a certain plane or a certain straight line, the system falls into a singular state.

According to different combinations of gimbal angles, singularities can be divided into elliptic singularities and hyperbolic singularities. Elliptic singularities include internal elliptic singularities and external saturation singularities. Hyperbolic singularities include nondegenerate hyperbolic singularities and degenerate hyperbolic singularities. Elliptic singularity and degenerate hyperbolic singularity are not passable or they cannot be escaped by null motion [2], [25], [27]. Singular surfaces are a set of points in angular momentum space corresponding to one singular gimbal angle at least. It can help satellite attitude-control designer to know all angular momenta that risk a singular Jacobian a-priori so that he or she may design an algorithm to escape or avoid such points [26]. The singular surfaces of the pyramid array are shown in Fig. 3.

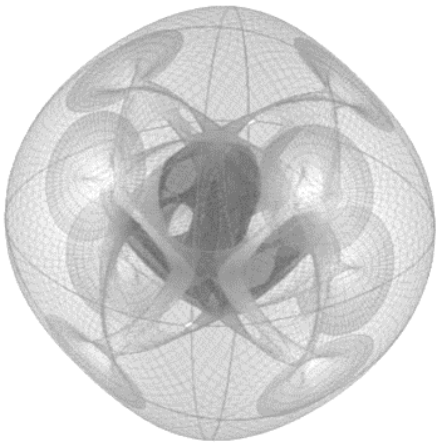

FIGURE 3. Singular surfaces in angular momentum space for four SGCMG pyramid array (Cited from reference [26]).

In SGCMGs with redundant design, such as the pyramid configurations, the mapping from gimbal angular space to angular momentum space is multi-shot except for the boundary of momentum envelope [2], [19], [26], [27]. Therefore, we think all the singular surfaces except the outermost singular surface are possibly passable. An example is given as follows:

$$\begin{cases} \boldsymbol{\delta} = \begin{pmatrix} \delta_1 & \delta_2 & \delta_3 & \delta_4 \end{pmatrix}^T \\ \boldsymbol{\delta}_{\mathrm{a}}^{\mathrm{s}} = \begin{pmatrix} \delta_{\mathrm{a1}}^{\mathrm{s}} & \delta_{\mathrm{a2}}^{\mathrm{s}} & \delta_{\mathrm{a3}}^{\mathrm{s}} & \delta_{\mathrm{a4}}^{\mathrm{s}} \end{pmatrix}^T \\ \mathbf{H}_{\mathrm{a}} = \begin{pmatrix} h_{\mathrm{ax}} & h_{\mathrm{ay}} & h_{\mathrm{az}} \end{pmatrix}^T \\ \mathbf{H}(\boldsymbol{\delta}) = \mathbf{h}_1(\delta_1) + \mathbf{h}_2(\delta_2) + \mathbf{h}_3(\delta_3) + \mathbf{h}_4(\delta_4) = \mathbf{H}_{\mathrm{a}} \end{cases} \tag{3}$$

Suppose $\boldsymbol{\delta}_{\mathrm{a}}^{\mathrm{s}}$ is corresponding to an internal elliptic singularity, and $\mathbf{H}_{\mathrm{a}}$ is the angular momentum corresponding to $\boldsymbol{\delta}_{\mathrm{a}}^{\mathrm{s}}$. Due to (3) is undetermined, the number of $\boldsymbol{\delta}$ satisfying $\mathbf{H}(\boldsymbol{\delta}) = \mathbf{H}_{\mathrm{a}}$ is infinite. However, there is no theory that can directly judge whether an infinite number of $\boldsymbol{\delta}$ values are singular. In the infinite number of values of $\boldsymbol{\delta}$, $\mathbf{H}_{\mathrm{a}}$ is locally passable [26] as long as there is one value corresponding to a non-singular state or non-degenerate hyperbolic singularity. An excellent steering law should have the ability to pass through this type of singular surface. The following simulation experiment (Fig. 30) verifies that the proposed steering law can pass though such a singular surface.

C. GENERAL FORM OF STEERING LAW BASED ON SINGULAR VALUE DECOMPOSITION

$$\boldsymbol{\tau}_{\mathrm{d}} = h_0 \mathbf{J} \dot{\boldsymbol{\delta}} \tag{4}$$

Refer to (2), in order to output the desired torque $\boldsymbol{\tau}_{\mathrm{d}}$, the command angular velocity of the gimbal motor should be solved from (4). According to the singular value decomposition theory, $\mathbf{J}$ can be decomposed into the product of three matrices, that is $\mathbf{J} = \mathbf{USV}^T$ where $\mathbf{U} = \begin{pmatrix}\hat{\mathbf{u}}_1 & \hat{\mathbf{u}}_2 & \hat{\mathbf{u}}_3\end{pmatrix}$ and $\mathbf{V} = \begin{pmatrix}\hat{\mathbf{v}}_1 & \hat{\mathbf{v}}_2 & \hat{\mathbf{v}}_3 & \hat{\mathbf{v}}_4\end{pmatrix}$. U and V are 3×3 and 4×4 unitary matrix, respectively. $\mathbf{S}$ is a 3×4 matrix. Suppose $rank(\mathbf{J}) = 3$, $\dot{\boldsymbol{\delta}}$ can be derived as follows.

$$\begin{cases} \mathbf{S} = \begin{pmatrix} \sigma_1 & 0 & 0 & 0 \\ 0 & \sigma_2 & 0 & 0 \\ 0 & 0 & \sigma_3 & 0 \end{pmatrix} \quad \mathbf{S}^* = \begin{pmatrix} \dfrac{1}{\sigma_1} & 0 & 0 \\ 0 & \dfrac{1}{\sigma_2} & 0 \\ 0 & 0 & \dfrac{1}{\sigma_3} \\ 0 & 0 & 0 \end{pmatrix} \\ \boldsymbol{\tau}_{\mathrm{d}} = h_0 \mathbf{J}\dot{\boldsymbol{\delta}} = h_0 \mathbf{USV}^T \dot{\boldsymbol{\delta}} \\ \Rightarrow \dot{\boldsymbol{\delta}} = \dfrac{1}{h_0}\mathbf{VS}^*\mathbf{U}^T\boldsymbol{\tau}_{\mathrm{d}} = \dfrac{1}{h_0}\sum_{i=1}^{3}\hat{\mathbf{v}}_i\dfrac{1}{\sigma_i}\hat{\mathbf{u}}_i^T\boldsymbol{\tau}_{\mathrm{d}} \\ \quad = \dfrac{\hat{\mathbf{v}}_1}{h_0\sigma_1}\boldsymbol{\tau}_{\mathrm{du1}} + \dfrac{\hat{\mathbf{v}}_2}{h_0\sigma_2}\boldsymbol{\tau}_{\mathrm{du2}} + \dfrac{\hat{\mathbf{v}}_3}{h_0\sigma_3}\boldsymbol{\tau}_{\mathrm{du3}} \\ \quad = \dot{\boldsymbol{\delta}}_{\mathrm{du1}} + \dot{\boldsymbol{\delta}}_{\mathrm{du2}} + \dot{\boldsymbol{\delta}}_{\mathrm{du3}} \end{cases} \tag{5}$$

Fig. 4a is the geometric interpretation of equation (5) $\hat{\mathbf{u}}_1$, $\hat{\mathbf{u}}_2$, $\hat{\mathbf{u}}_3$constitute a set of orthogonal basis in three-dimensional space, and $\boldsymbol{\tau}_{d\mathbf{ui}} = \hat{\mathbf{u}}_i^T\boldsymbol{\tau}_{\mathrm{d}}$ denotes the coordinates of $\boldsymbol{\tau}_d$. $\hat{\mathbf{v}}_i/(h_0\sigma_i)$ is the angular speed of the gimbal motors which can make the SGCMGs output the unit torque along $\hat{\mathbf{u}}_i$. Fig. 4b shows the relationship between $\dot{\boldsymbol{\delta}}$, $\hat{\mathbf{v}}_i$, $\boldsymbol{\tau}_{out}$, σ_i, and $\hat{\mathbf{u}}_i$ from another aspect. $\hat{\mathbf{v}}_4$ is the basis of the null space of $\mathbf{J}$, that is $h_0\mathbf{J}\hat{\mathbf{v}}_4 = h_0\mathbf{USV}^T\hat{\mathbf{v}}_4 = 0$. It is also known as the solution of zero-motion. Based on aforementioned analysis, the general form of $\dot{\boldsymbol{\delta}}$ which is solved from (4) is expressed as follows:

$$\begin{cases} \dot{\boldsymbol{\delta}}_\tau = \dfrac{1}{h_0}\sum_{i=1}^{3}\hat{\mathbf{v}}_i\dfrac{1}{\sigma_i}\hat{\mathbf{u}}_i^T\boldsymbol{\tau}_d \\ \hat{\dot{\boldsymbol{\delta}}}_z = \hat{\mathbf{v}}_4 \\ \dot{\boldsymbol{\delta}} = \dot{\boldsymbol{\delta}}_\tau + \lambda\hat{\dot{\boldsymbol{\delta}}}_z \end{cases} \tag{6}$$

where λ is an arbitrary constant.

III. A BRIEF INTRODUCTION AND ANALYSIS OF SOME TYPICAL STEERING LAWS BASED ON THE ABOVE THEORETICAL FRAMEWOK

A. SINGUL·ARITY MEASUREMENT

Singularity measurement is used to measure the singularity of the system. The smaller the singularity measure is, the more likely the system falls into singularity. At present, there are mainly two singular measurement methods, one is using σ_3 to measure the singularity, the other is using $\sqrt{\det\left(\mathbf{JJ}^T\right)}$ to measure the singularity.

σ_3 is the smallest singular value, refer to Fig. 4b, the singular state of the pyramid configured SGCMGs system means $\sigma_3 = 0$. Therefore, σ_3 has been used as a singular metric for

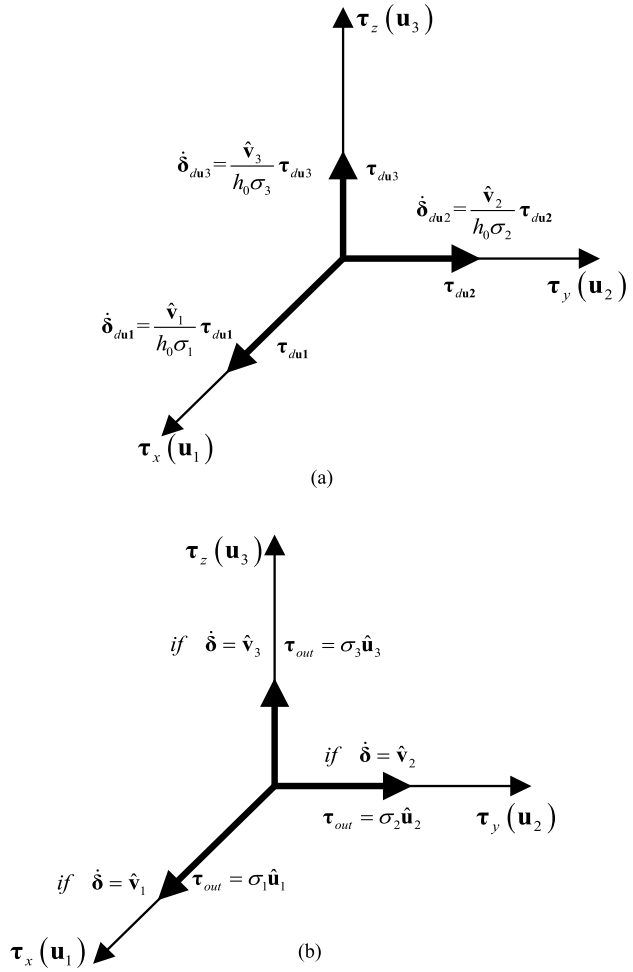

FIGURE 4. (a) The Geometric interpretation of (5). (b) The Geometric interpretation of U, S, V.

SGCMGs in many documents. This is the most intuitive way to measure singularity.

$\sqrt{\det\left(\mathbf{JJ}^T\right)}$ equals to $\sigma_1\sigma_2\sigma_3$. As shown in Fig. 4b, it represents the volume of a geometry. When the system approaches singularity, the geometric body will be flattened and the volume will be reduced. When the system falls into singularity, the geometric body will be compressed into a plane and the volume will be zero.

B. NON-DIRECTIONAL NULL-MOTION ALGORITHM

$$\begin{cases} \dot{\boldsymbol{\delta}}_{ND} = \dot{\boldsymbol{\delta}}_\tau + \lambda\dot{\boldsymbol{\delta}}_z = \dfrac{1}{h_0}\sum_{i=1}^{3}\hat{\mathbf{v}}_i\dfrac{1}{\sigma_i}\hat{\mathbf{u}}_i^T\boldsymbol{\tau}_d + \lambda\hat{\mathbf{v}}_4 \\ \lambda\left(\hat{\delta}\right) = \begin{cases} m^6 & if\ m \geq 1 \\ m^{-6} & if\ m < 1 \end{cases} \\ m = \sigma_1\sigma_2\sigma_3 \end{cases} \tag{7}$$

This is a torque error free singularity avoidance steering law and it was proposed in reference [4]. This method adds null motion directly according to the singular measure value of

the system as shown in (7). It is not easy to fall into local extremum and it can avoid an internal elliptic singularity. However, there are two obvious drawbacks of this steering law. One is that substantial null motion is introduced even when the system is far from being singular. This will not only result in the waste of system resources, but also make the system close to singularity [4]. The other one is that this method adds null motion only according to the singularity measure of the system, without considering whether null motion is effective or not. These two defects directly weaken the singularity avoidance ability of this steering law.

C. OFF-DIAGONAL SINGULARITY-ROBUST STEERING LAW

$$\dot{\boldsymbol{\delta}}_{ODSR} = \frac{1}{h_0}\mathbf{W}\mathbf{J}^T\left[\mathbf{J}\mathbf{W}\mathbf{J}^T + \mathbf{V}\right]^{-1}\boldsymbol{\tau}_d \tag{8}$$

$$\mathbf{W} = \begin{pmatrix} w_1 & \mu & \mu & \mu \\ \mu & w_2 & \mu & \mu \\ \mu & \mu & w_3 & \mu \\ \mu & \mu & \mu & w_4 \end{pmatrix} > 0 \tag{9}$$

$$\mathbf{V} = \mu\begin{pmatrix} 1 & \varepsilon_3 & \varepsilon_2 \\ \varepsilon_3 & 1 & \varepsilon_1 \\ \varepsilon_2 & \varepsilon_1 & 1 \end{pmatrix} > 0 \tag{10}$$

$$\mu = \mu_0 \exp(-\kappa \det\left(\mathbf{J}\mathbf{J}^T\right)) \tag{11}$$

$$\varepsilon_i = \varepsilon_0 \sin\left(wt + \phi_i\right) \tag{12}$$

This is a hybrid steering law, which has excellent ability to escape from the singularities [12]. $\mathbf{W}$ helps the system to avoid singularity. $\mathbf{V}$ makes (8) generate deterministic dither signals, thus enabling the system to have excellent singularity escape capability. However, the parameters w_i, μ_0, ε_0, w, κ, and ϕ_i are selected by trial and error for each maneuver. The ODSR method is more suitable to be used for maneuvers known in advance, which are tuned and tested to ensure feasibility. This makes it difficult to use in practice [12], [23].

D. DIRECTIONAL SINGULARITY ESCAPE AND AVOIDENCE STEERING LAW

$$\begin{aligned}\dot{\boldsymbol{\delta}}_{dsea} &= \frac{1}{h_0}\mathbf{J}^T(\mathbf{J}\mathbf{J}^T + \alpha\hat{\mathbf{u}}_3\hat{\mathbf{u}}_3^T)^{-1}\boldsymbol{\tau}_d \\ &\quad + \left(\mathbf{I}_4 - \mathbf{J}^T(\mathbf{J}\mathbf{J}^T + \alpha\hat{\mathbf{u}}_3\hat{\mathbf{u}}_3^T)^{-1}\mathbf{J}\right)\dot{\boldsymbol{\delta}}_s \\ &= \frac{1}{h_0}\left(\frac{1}{\sigma_1}\hat{\mathbf{v}}_1\hat{\mathbf{u}}_1^T + \frac{1}{\sigma_2}\hat{\mathbf{v}}_2\hat{\mathbf{u}}_2^T + \frac{\sigma_3}{\sigma_3^2+\alpha}\hat{\mathbf{v}}_3\hat{\mathbf{u}}_3^T\right)\boldsymbol{\tau}_d \\ &\quad + \left(\frac{\alpha}{\sigma_3^2+\alpha}\hat{\mathbf{v}}_3\hat{\mathbf{v}}_3^T + \hat{\mathbf{v}}_4\hat{\mathbf{v}}_4^T\right)\dot{\boldsymbol{\delta}}_s\end{aligned} \tag{13}$$

$$\alpha = \sigma_{\min}^2 e^{\eta\left(\sigma_{\min}^2 - \sigma_3^2\right)} \tag{14}$$

This hybrid steering law was proposed in reference [23], α is a function of σ_3. $\dot{\boldsymbol{\delta}}_s$ is the desired angular velocity used to avoid or escape singularity. η is a scale factor. $\sigma_{\min}$ is a constant. When $\sigma_3 \gg \sigma_{\min}$, $\alpha \to 0$, (13) becomes (15). Equation (15) is a singularity avoidance steering law based on zero motion.

$$\dot{\boldsymbol{\delta}}_{desa} = \frac{1}{h_0}\left(\frac{1}{\sigma_1}\hat{\mathbf{v}}_1\hat{\mathbf{u}}_1^T + \frac{1}{\sigma_2}\hat{\mathbf{v}}_2\hat{\mathbf{u}}_2^T + \frac{1}{\sigma_3}\hat{\mathbf{v}}_3\hat{\mathbf{u}}_3^T\right)\boldsymbol{\tau}_d + \hat{\mathbf{v}}_4\hat{\mathbf{v}}_4^T\dot{\boldsymbol{\delta}}_s \tag{15}$$

When $\sigma_3 \ll \sigma_{\min}$, the system is close to a singular state, meanwhile $\sigma_3/\alpha \to 0$, $\sigma_3/\left(\sigma_3^2+\alpha\right) \to 0$, $\alpha/\left(\sigma_3^2+\alpha\right) \to 1$. On this condition, (13) becomes (16), the system cannot output the torque along $\hat{\mathbf{u}}_3$, and $\hat{v}_3$ is also used as a part of null motion, which increases the possibility of singularity avoidance and escape.

$$\dot{\boldsymbol{\delta}}_{desa} = \frac{1}{h_0}\left(\frac{1}{\sigma_1}\hat{\mathbf{v}}_1\hat{\mathbf{u}}_1^T + \frac{1}{\sigma_2}\hat{\mathbf{v}}_2\hat{\mathbf{u}}_2^T\right)\hat{\boldsymbol{\tau}}_d + \left(\hat{\mathbf{v}}_3\hat{\mathbf{v}}_3^T + \hat{\mathbf{v}}_4\hat{\mathbf{v}}_4^T\right)\dot{\boldsymbol{\delta}}_s \tag{16}$$

$\dot{\boldsymbol{\delta}}_s$ is the desired gimbal angular velocity that need to be carefully designed to help the system to avoid the singularities. The design of $\dot{\boldsymbol{\delta}}_s$ is the core of DSEA steering law. For a detailed description of this design method, please refer to reference [23]. Here we briefly list the design method of $\dot{\boldsymbol{\delta}}_s$. σ_{acp}, $\tau_{\max}$, and $\tau_{\min}$ are constants.

$$\mathbb{I} = \left\{i|\hat{\mathbf{h}}_i^T\boldsymbol{\tau}_d > 0\right\} \tag{17}$$

$${}^{RA}\hat{\mathbf{f}}_i = \begin{cases} \dfrac{\hat{\mathbf{g}}_i \times \hat{\boldsymbol{\tau}}_d}{\left\|\hat{\mathbf{g}}_i \times \hat{\boldsymbol{\tau}}_d\right\|} & if\ \hat{\mathbf{h}}_i^T\boldsymbol{\tau}_d > 0 \\ -\dfrac{\hat{\mathbf{g}}_i \times \hat{\boldsymbol{\tau}}_d}{\left\|\hat{\mathbf{g}}_i \times \hat{\boldsymbol{\tau}}_d\right\|} & if\ \hat{\mathbf{h}}_i^T\boldsymbol{\tau}_d < 0 \end{cases} \tag{18}$$

$$\begin{cases} k_j = \sigma_{acp}^2 e^{\eta\left(\sigma_{acp}^2 - \sigma_j^2\right)} \\ z_j = \dfrac{\sigma_j^2}{\sigma_j^2 + k_j} \\ \delta_{track} = 1 - \sqrt{\sum_{j=1}^{3}(1-z_j)^2(\hat{\mathbf{u}}_j^T\hat{\boldsymbol{\tau}}_d)^2} \end{cases} \tag{19}$$

$$\left|\dot{\boldsymbol{\delta}}_{s,i}\right| = d_0\left\|\frac{\boldsymbol{\tau}_d}{\tau_{\max}}\right\|^{\xi}\frac{\|\boldsymbol{\tau}_d\|^3}{\|\boldsymbol{\tau}_d\|^3 + \tau_{\min}^3}d_i\left(1-\delta_{track}\right) \tag{20}$$

$$d_i = \left(\max\left(\hat{h}_i^T\hat{\boldsymbol{\tau}}_d, 0\right)\right)^2 \tag{21}$$

$${}^{RA}\left|\dot{\delta}_{s,i}\right| = \begin{cases} d_0\left\|\dfrac{\boldsymbol{\tau}_d}{\tau_{\max}}\right\|^{\xi}\dfrac{\|\boldsymbol{\tau}_d\|^3}{\|\boldsymbol{\tau}_d\|^3 + \tau_{\min}^3} & if\ \hat{\mathbf{h}}_i^T\tau_d > 0 \\ \cdot\left(\boldsymbol{\tau}_d^T\boldsymbol{\tau}_d - \left(\mathbf{g}_i^T\boldsymbol{\tau}_d\right)^2\right) & \\ 0 & otherwise \end{cases} \tag{22}$$

$$\boldsymbol{\theta} = \begin{bmatrix}\theta_1 & \theta_2 & \theta_3 & \theta_4\end{bmatrix} \quad \theta_i \in \{-1, 0, 1\} \tag{23}$$

$${}^{RA}\boldsymbol{\tau}_s(\boldsymbol{\theta}) = \sum_{\mathbb{I}} h_i\theta_i{}^{RA}\hat{\mathbf{f}}_i{}^{RA}\left|\dot{\delta}_{s,i}\right| \tag{24}$$

$$\tilde{\boldsymbol{\theta}} = \arg\min\left\|{}^{RA}\boldsymbol{\tau}_s(\boldsymbol{\theta})\right\| \tag{25}$$

$$\dot{\boldsymbol{\delta}}_{\mathbf{s}}(\boldsymbol{\theta}) = \begin{bmatrix}\theta_1\left|\dot{\delta}_{s,1}\right| & \theta_2\left|\dot{\delta}_{s,2}\right| & \theta_3\left|\dot{\delta}_{s,3}\right| & \theta_4\left|\dot{\delta}_{s,4}\right|\end{bmatrix} \tag{26}$$

This steering law operates with less moment error, less delay in singularity escape, and lower peak gimbal rates,

Algorithm 1 Selecting Optimal $\dot{\boldsymbol{\delta}}_{\mathbf{s}}$

if $\mathbb{I} = \emptyset$ or $\|\boldsymbol{\tau}_d\| < \tau_{\min}$, **then** ▷ Eq. (17)
  $\dot{\boldsymbol{\delta}}_s = \mathbf{0}$
else
  for all $i \in \mathbb{I}$, **do**
    Evaluate ${}^{RA}\hat{\mathbf{f}}_i$, $\left|\dot{\boldsymbol{\delta}}_{s,i}\right|$, and ${}^{RA}\left|\dot{\boldsymbol{\delta}}_{s,i}\right|$ ▷ Eq. (18), (20) and (22)
  for all $2^{n_{anti}}$ possible vectors $\boldsymbol{\theta}$, do
    Evaluate $\left\|{}^{RA}\boldsymbol{\tau}_{\mathbf{s}}(\theta)\right\|$ ▷ Eq. (25)
  From these options, take $\tilde{\boldsymbol{\theta}} = \arg\min \left\|{}^{RA}\boldsymbol{\tau}_{\mathbf{s}}(\boldsymbol{\theta})\right\|$
  $\boldsymbol{\theta}^* = \text{PreventChattering}\left(\tilde{\boldsymbol{\theta}}\right)$ ▷ Algorithm 2
  $\dot{\boldsymbol{\delta}}_{\mathbf{s}} = \dot{\boldsymbol{\delta}}_{\mathbf{s}}\left(\boldsymbol{\theta}^*\right)$ ▷ Eq. (26)

Algorithm 2 Evaluation of $\boldsymbol{\theta}^* = \text{PreventChattering}\left(\tilde{\boldsymbol{\theta}}\right)$

Denote $\Delta = \left\|{}^{RA}\boldsymbol{\tau}_{\mathbf{s}}\left(\tilde{\boldsymbol{\theta}}\right)\right\| - \left\|{}^{RA}\boldsymbol{\tau}_{\mathbf{s}}\left(\boldsymbol{\theta}^*_{t_{k-1}}\right)\right\|$
if $\mathbb{I}_{t_k} = \mathbb{I}_{t_{k-1}}$, and $|\Delta| < \tau_{\min}$, then
  $\boldsymbol{\theta}^*_{t_k} = \boldsymbol{\theta}^*_{t_{k-1}}$
else
  if $\left\|\dot{\boldsymbol{\delta}}_s\left(\tilde{\boldsymbol{\theta}}\right) - \dot{\boldsymbol{\delta}}_{s,t_{k-1}}\right\| < \left\|\dot{\boldsymbol{\delta}}_s\left(\tilde{\boldsymbol{\theta}}\right) + \dot{\boldsymbol{\delta}}_{s,t_{k-1}}\right\|$, then
    $\boldsymbol{\theta}^*_{t_k} = \tilde{\boldsymbol{\theta}}$
  else
    $\boldsymbol{\theta}^*_{t_k} = -\tilde{\boldsymbol{\theta}}$

without tuning the controller separately for each maneuver. In addition, this method can efficiently deal with all types of singularities, using a single set of control parameters that can be selected based on physical and intuitive considerations. However, the strong singularity avoidance ability of this steering law depends partly on the introduction of torque error, which sacrifices the control accuracy.

$\dot{\boldsymbol{\delta}}_s$ is used to enhance the singularity avoidance ability of the system. However, in the process of designing $\dot{\boldsymbol{\delta}}_s$, there was no overall consideration combined with the information of $1/h_0\mathbf{J}^T(\mathbf{J}\mathbf{J}^T + \alpha\hat{\mathbf{u}}_3\hat{\mathbf{u}}_3^T)^{-1}\boldsymbol{\tau}_d$. This will result in a relatively small improvement in the ability of avoiding or escaping the singularity of the system, because part of the addition from $\dot{\boldsymbol{\delta}}_s$ is likely to be offset by $1/h_0\mathbf{J}^T(\mathbf{J}\mathbf{J}^T + \alpha\hat{\mathbf{u}}_3\hat{\mathbf{u}}_3^T)^{-1}\boldsymbol{\tau}_d$.

$$\begin{aligned}\mathbf{e} &= \boldsymbol{\tau}_d - \boldsymbol{\tau}_{out} = \boldsymbol{\tau}_d - h_0\mathbf{J}\dot{\delta}_{desa} \\ &= \frac{\alpha}{\sigma_3^2 + \alpha}\left(\hat{\mathbf{u}}_3^T\tau_d - h_0\sigma_3\hat{\mathbf{v}}_3^T\dot{\boldsymbol{\delta}}_s\right)\hat{\mathbf{u}}_3 \end{aligned} \tag{27}$$

According to [23], the torque error of this steering law is expressed as (27). If α is a constant equal to zero, the norm of $\mathbf{e}$ will also be equal to zero, under which condition (13) will be converted to (15). Equation (15) is a simple steering law similar to the local gradient method [4], [22], and it does not have good singularity avoidance ability. If α is defined as (14), the value of torque error under this condition is related to (14) and is no longer equal to zero. Therefore, it can be considered that the excellent singularity avoidance capability of DSEA steering law is obtained at the expense of the accuracy of output torque.

IV. VECTOR CONTROL BASED STEERING LAW DESIGN

A. EFFECTIVE RESIDUAL ANGULAR MOMENTUM EVALUATION

The concept of effective residual angular momentum evaluation for each SGCMG of command torque is similar to the concept of gimbal potential which is proposed in [23]. However, in reference [23], the gimbal potential is only used to judge whether the angular momentum of the system is saturated. Inspired by this idea, we design a novel evaluation measure with similar function in reference [23] and further expand the application of this measure.

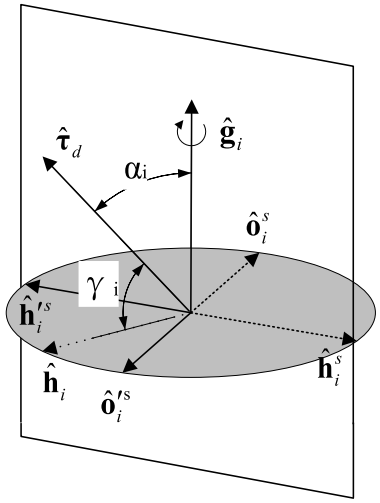

FIGURE 5. SGCMG singular state diagram.

In Fig. 5, $\hat{\mathbf{o}}_i^s$ and $\hat{\mathbf{o}}_i'^s$ are collinear, $\hat{\mathbf{h}}_i'^s$, $\hat{\boldsymbol{\tau}}_d$, $\hat{\mathbf{g}}_i$, and $\hat{\mathbf{h}}_i^s$ are all located in the plane perpendicular to $\hat{\mathbf{o}}_i^s$ and $\hat{\mathbf{o}}_i'^s$. The characters $\hat{\mathbf{g}}_i$, $\hat{\boldsymbol{\tau}}_d$, and $\hat{\mathbf{h}}_i$ represent the gimbal axis, direction of the desired torque, and real-time orientation of rotor angular momentum, respectively. The characters $\hat{\mathbf{h}}_i^s$ and $\hat{\mathbf{h}}_i'^s$ indicate saturation singular locations and internal singular locations of rotor angular momentum corresponding to $\hat{\boldsymbol{\tau}}_d$, respectively. If the gimbal motor rotates clockwise as indicated in the figure, the output torques corresponding to $\hat{\mathbf{h}}_i^s$ and $\hat{\mathbf{h}}_i'^s$ are along $\hat{\mathbf{o}}_i^s$ and $\hat{\mathbf{o}}_i'^s$. $\hat{\mathbf{o}}_i^s$ and $\hat{\mathbf{o}}_i'^s$ are perpendicular to $\hat{\boldsymbol{\tau}}_d$. Angle α_i is the acute or right angle between $\hat{\boldsymbol{\tau}}_d$ and the straight line where $\hat{\mathbf{g}}_i$ lies, it ranges from 0 to $\pi/2$. Angle γ_i is the angle between $\hat{\mathbf{h}}_i$ and $\hat{\boldsymbol{\tau}}_d$ which ranges from $\pi/2-\alpha_i$ to $\pi/2+\alpha_i$. The interval length of γ_i is $\pi/2+\alpha_i-(\pi/2-\alpha_i) = 2\alpha_i$, where $2\alpha_i$ belongs to 0 to π. For $\hat{\boldsymbol{\tau}}_d$, we use $2\alpha_i/\pi$ to evaluate the maximum effective angular momentum reserve each SGCMG can have.

SGCMG is an angular momentum exchange component. If SGCMG outputs the torque in the direction of $\hat{\boldsymbol{\tau}}_d$, then the final position of $\hat{\mathbf{h}}_i$ is $\hat{\mathbf{h}}_i^s$, where $\gamma_i = \pi/2 + \alpha_i$, and the remaining effective angular momentum reserve of the SGCMG for $\hat{\boldsymbol{\tau}}_d$ is 0%. If $\hat{\mathbf{h}}_i$ is located at $\mathbf{h}'^s_i$, then $\gamma_i = \pi/2 - \alpha_i$, the remaining effective angular momentum reserve of the SGCMG for $\hat{\boldsymbol{\tau}}_d$ is 100%.

In order to avoid the internal singular state of SGCMGs, $\hat{\mathbf{h}}_i$ should rotate away from $\mathbf{h}'^s_i$ and towards $\hat{\mathbf{h}}_i^s$ to avoid

approaching or stopping at $\hat{\mathbf{h}}_i'^s$. We use the value of γ_i to express the change of $\hat{\mathbf{h}}_i$ relative to $\hat{\boldsymbol{\tau}}_d$. The angular distance between γ_i and its maximum value $\pi/2+\alpha_i$ is $\pi/2+\alpha_i-\gamma_i$. Because the interval length of the value range of γ_i is $2\alpha_i$, we use $(\pi/2+\alpha_i-\gamma_i)/(2\alpha_i)$ to represent the proportion of the remaining angular distance to the value range of γ_i. Combined with the maximum effective angular momentum of each SGCMG $(2\alpha_i/\pi)$, the complete expression to evaluating the effective residual angular momentum of a single SGCMG is as (28).

$$eram_i = \frac{\frac{1}{2}\pi+\alpha_i-\gamma_i}{2\alpha_i}\frac{2\alpha_i}{\pi} = \frac{\frac{1}{2}\pi+\alpha_i-\gamma_i}{\pi} \tag{28}$$

According to (28), if $\hat{\mathbf{h}}_i$ is located at $\hat{\mathbf{h}}_i'^s$, then $\gamma_i = \pi/2-\alpha_i$, $eram_i$ takes the maximum value equals to $2\alpha_i/\pi$. If $\hat{\mathbf{h}}_i$ is located at $\mathbf{h}_i^s$, then $\gamma_i = \pi/2+\alpha_i$, $eram_i$ takes the minimum value equals to 0. If $\alpha_i = 0$, then $\gamma_i = \pi/2$, $eram_i = 0$, any rotation of this SGCMG cannot produce any torque component along $\hat{\boldsymbol{\tau}}_d$.

B. SYSTEM STATE EVALUTATION

The residual resources of SGCMGs system can be evaluated by $rrss = \sum_i eram_i$ [23]. When $rrss \to 0$, the angular momentum resources of the system will be exhausted. In such a situation, if $\sigma_3 \gg 0$, the system can continue to run without singularity, and *rrss* continues to approach zero until σ_3 approaches zero. Because both *rrss* and σ_3 are approaching zero, the angular momentum of the system has reached saturation. Under this condition, the system should stop outputting $\boldsymbol{\tau}_d$ and start the desaturation control scheme. When σ_3 approaches zero, the system will encounter singularity. If the value of *rrss* is still large, the system will encounter an internal singularity. It is valuable to escape the singularity under this assumption. If the value of *rrss* is already small or equal to zero, the system will encounter internal singularity nears external saturation singularity or external saturation singularity. It is meaningless to escape singularity under this assumption. The above analysis can be summarized as (29).

$$sse = rrss + \sigma_3 \times \begin{cases} sse > \varepsilon_1 & \textit{Sufficient angular momentum reserve} \\ \varepsilon < sse < \varepsilon_1 & \textit{In the middle} \\ sse < \varepsilon & \textit{Angular momentum reserves are exhausted} \end{cases} \tag{29}$$

ε and ε_1 are the constants. *sse* is used to evaluate the total momentum state of the system. The larger ε is, the smaller the available angular momentum envelope is.

C. DESIGN OF DESIRED GIMBAL ANGULAR VELOCITY

In order to output the desired torque $\boldsymbol{\tau}_d$, each SGCMG's momentum tends to rotate from $\mathbf{h}_i'^s$ to $\mathbf{h}_i^s$ [3], [6], [23]. If the SGCMG with more effective residual angular momentum is assigned a larger gimbal angular velocity toward the saturation singularity direction, the possibility of the system falling into singularity will be reduced. Based on this idea, we design vector $\hat{\mathbf{G}}$, which gives the expected relationship between the gimbal angular velocities of each SGCMG in (30).

$$\begin{cases} f_i = \begin{cases} 0.01 & \textit{if } \hat{\mathbf{h}}_i = \hat{\mathbf{h}}_i'^s \textit{ and } \dot{\delta}_i = 0 \\ \dfrac{\left|\hat{\mathbf{h}}_i\cdot\hat{\mathbf{o}}_i'^s + d\right| - \left|\hat{\mathbf{h}}_i\cdot\hat{\mathbf{o}}_i'^s - d\right|}{2d} & \textit{otherwise} \end{cases} \\ \mathbf{n} = \begin{pmatrix} f_1 e^{\xi * eram_1} \\ f_2 e^{\xi * eram_2} \\ f_3 e^{\xi * eram_3} \\ f_4 e^{\xi * eram_4} \end{pmatrix} \\ \hat{\mathbf{G}} = \begin{cases} \mathbf{n}/\|\mathbf{n}\| & \textit{if } \|\mathbf{n}\| \neq 0 \\ 0 & \textit{if } \|\mathbf{n}\| = 0 \end{cases} \end{cases} \tag{30}$$

Each element in $\mathbf{n}$ is the product of $e^{\xi * eram_i}$ and f_i. $e^{\xi * eram_i}$ gives the amplitude of the gimbal angular velocity where ξ is a stretching factor greater than 1. The exponential form of $eram_i$ can enhance the singularity avoidance ability of the system. f_i gives the rotational direction. f_i equals -1 for clockwise rotation and f_i equals 1 for counterclockwise rotation. In order to avoid the influence caused by the jump of its value, we make it to take values continuously from -1 to 1. When $\left|\hat{\mathbf{h}}_i\cdot\hat{\mathbf{o}}_i'^s\right| > d, f_i = sign\left(\hat{\mathbf{h}}_i\cdot\hat{\mathbf{o}}_i'^s\right)$. when $\left|\hat{\mathbf{h}}_i\cdot\hat{\mathbf{o}}_i'^s\right| < d$, $f_i = \hat{\mathbf{h}}_i\cdot\hat{\mathbf{o}}_i'^s/d$. d is a positive constant. This design can prevent the jump of $\mathbf{n}$ caused by $\hat{\mathbf{h}}_i$ passing through $\hat{\mathbf{h}}_i'^s$. However, the above design will cause another problem. If a certain $\hat{\mathbf{h}}_i$ happens to be located at $\hat{\mathbf{h}}_i'^s$, then unless $\boldsymbol{\tau}_d$ is parallel to $\hat{\mathbf{g}}_i$, $e^{\xi * eram_i}$ is greater than one. However, at this time $\hat{\mathbf{h}}_i\cdot\hat{\mathbf{o}}_i'^s = 0$, and then f_i is equal to zero, the information brought by $e^{\xi * eram_i}$ will be completely erased by the multiplication of f_i. Under the above conditions, if the rotating speed of the SGCMG is not zero, $\hat{\mathbf{h}}_i$ will normally pass through $\hat{\mathbf{h}}_i'^s$, and the influence of f_i being equal to zero will not be too great. If the rotating speed of the SGCMG $(\dot{\delta}_i)$ is exactly equals to zero, f_i being equal to zero will easily make $\hat{\mathbf{h}}_i$ stuck at $\hat{\mathbf{h}}_i'^s$. In order to avoid the above unfavorable situation and ensure the continuity of f_i as much as possible, when $\hat{\mathbf{h}}_i = \hat{\mathbf{h}}_i'^s$ and $\dot{\delta}_i = 0, f_i$ is forced to be equal to 0.01.

D. SINGULARITY AVOIDENCE CONTROL STRATEGY

Inspired by the references [3] and [6], we propose a novel singularity avoidance control strategy that only depends on adding zero motion. Using moment motion $\dot{\boldsymbol{\delta}}_\tau$ and reference quantity $\hat{\mathbf{G}}$, we derive a new zero motion addition formula. In addition, we also deeply analyzed the influence of zero motion amplitude on the algorithm performance from the perspective of geometry, and proposed a new adaptive zero motion amplitude limitation method. These core innovations will make our algorithm achieve good performance.

According to (6), $\dot{\boldsymbol{\delta}}$ can be decomposed into $\dot{\boldsymbol{\delta}}_\tau$ and $\lambda\hat{\dot{\boldsymbol{\delta}}}_z$, where λ is an arbitrary constant. The value of parameter λ can adjust the direction of $\dot{\boldsymbol{\delta}}$ to minimize the included angle

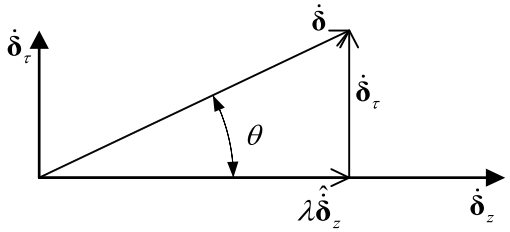

FIGURE 6. Pseudo-inverse solution and null-motion.

θ between $\dot{\boldsymbol{\delta}}$ and $\hat{\mathbf{G}}$.This strategy avoids the singularity of the system by selecting a suitable λ in real time. The schematic diagram of the geometric relationship between $\dot{\boldsymbol{\delta}}_\tau$, $\lambda\dot{\hat{\boldsymbol{\delta}}}_z$ and $\dot{\boldsymbol{\delta}}$ is shown in Fig. 6, where $\dot{\boldsymbol{\delta}}_\tau$ is perpendicular to $\lambda\dot{\hat{\boldsymbol{\delta}}}_z$. θ is defined by (31).

$$\theta = \arctan\left(\frac{\left\|\dot{\boldsymbol{\delta}}_\tau\right\|}{\left\|\lambda\dot{\hat{\boldsymbol{\delta}}}_z\right\|}\right) = \arctan\left(\frac{\dot{\delta}_\tau}{\lambda\dot{\hat{\delta}}_z}\right) == \arctan\left(\frac{\dot{\delta}_\tau}{\lambda}\right) \tag{31}$$

$$\frac{d\theta}{d\lambda} = \frac{-\left\|\dot{\boldsymbol{\delta}}_\tau\right\|}{\lambda^2 + \left\|\dot{\boldsymbol{\delta}}_\tau\right\|^2} \tag{32}$$

According to (31), the derivative of the included angleθ to λ is (32), and its norm becomes smaller and smaller with the increase of λ, that is, the larger the value of parameter λ, the weaker its ability to adjust the direction of $\dot{\boldsymbol{\delta}}$. For example, if λ changes from 0 to $\dot{\delta}_\tau$, θ changes from 90 to 45 degrees, λ continues to change from $\dot{\delta}_\tau$ to $10\dot{\delta}_\tau$, then θ changes from 45 to 5.71 degrees, finally λ changes from $10\dot{\delta}_\tau$ to infinity, and θ changes only from 5.71 to zero degree. Besides, there is a physical limit to the amplitude of the gimbal angular velocity, so it is of limited significance to take the amplitude of λ to infinity. More importantly, if λ takes the value to infinity, the slight change of θ between 5.71 to 0 degree will lead to the drastic change of λ, which will make the gimbal angular velocity given by the steering law unstable. Therefore, it is necessary to limit the magnitude of λ properly.

$$\lambda = \frac{\left\|\dot{\boldsymbol{\delta}}_\tau\right\|}{\hat{\mathbf{G}}\cdot\dot{\hat{\boldsymbol{\delta}}}_\tau}\hat{\mathbf{G}}\cdot\dot{\hat{\boldsymbol{\delta}}}_z\left(\hat{\mathbf{G}}\cdot\dot{\hat{\boldsymbol{\delta}}}_\tau > 0\right) \tag{33}$$

$$\lambda = \frac{\left\|\dot{\boldsymbol{\delta}}_\tau\right\|}{\max\left(\varsigma, \hat{\mathbf{G}}\cdot\dot{\hat{\boldsymbol{\delta}}}_\tau\right)}\hat{\mathbf{G}}\cdot\dot{\hat{\boldsymbol{\delta}}}_z\left(\hat{\mathbf{G}}\cdot\dot{\hat{\boldsymbol{\delta}}}_\tau > 0\right) \tag{34}$$

We determine the value of λ from the perspective of minimizing the angle between $\dot{\boldsymbol{\delta}}$ and $\hat{\mathbf{G}}$. If the angle between $\dot{\boldsymbol{\delta}}_\tau$ and $\hat{\mathbf{G}}$ is an acute angle, i.e. $\hat{\mathbf{G}}\cdot\dot{\hat{\boldsymbol{\delta}}}_\tau > 0$, the angle between $\dot{\boldsymbol{\delta}}$ and $\hat{\mathbf{G}}$ is the smallest when $\dot{\boldsymbol{\delta}}$ is at the orthographic projection position of $\hat{\mathbf{G}}$ on the plane spanned by $\dot{\boldsymbol{\delta}}_\tau$ and $\lambda\dot{\hat{\boldsymbol{\delta}}}_z$. In this case, the value of λ is determined by (33). Considering that it is necessary to limit the amplitude of λ, we modify (33) to (34), and ς is a constant greater than zero and less than one.

$$\lambda = \frac{\left\|\dot{\boldsymbol{\delta}}_\tau\right\|}{\max\left(\varsigma, -\hat{\mathbf{G}}\cdot\dot{\hat{\boldsymbol{\delta}}}_\tau\right)}\hat{\mathbf{G}}\cdot\dot{\hat{\boldsymbol{\delta}}}_z\left(\hat{\mathbf{G}}\cdot\dot{\hat{\boldsymbol{\delta}}}_\tau < 0\right) \tag{35}$$

If the angle between $\dot{\boldsymbol{\delta}}_\tau$ and $\hat{\mathbf{G}}$ is obtuse, i.e. $\hat{\mathbf{G}}\cdot\dot{\hat{\boldsymbol{\delta}}}_\tau < 0$, then $\dot{\boldsymbol{\delta}}_\tau$ and $\lambda\dot{\boldsymbol{\delta}}_z$ will no longer be able to form the projection of $\hat{\mathbf{G}}$ on the plane they determined. To ensure the continuity of the value of λ and considering the correlation between $\hat{\mathbf{G}}$ and $\dot{\hat{\boldsymbol{\delta}}}_z$, we design (35) to determine the value of λ. Equation (34) and (35) guarantee the continuity of λ together. In addition, $\hat{\mathbf{G}}\cdot\dot{\hat{\boldsymbol{\delta}}}_z$ measures the correlation between $\hat{\mathbf{G}}$ and $\dot{\hat{\boldsymbol{\delta}}}_z$. The bigger the value of $\left|\hat{\mathbf{G}}\cdot\dot{\hat{\boldsymbol{\delta}}}_z\right|$, the stronger the correlation between $\hat{\mathbf{G}}$ and $\dot{\hat{\boldsymbol{\delta}}}_z$. Finally, we integrate (34) and (35) into (36).

$$\lambda = \frac{\left\|\dot{\boldsymbol{\delta}}_\tau\right\|}{\max\left(\varsigma, \left|\hat{\mathbf{G}}\cdot\dot{\hat{\boldsymbol{\delta}}}_\tau\right|\right)}\hat{\mathbf{G}}\cdot\dot{\hat{\boldsymbol{\delta}}}_z \tag{36}$$

The purpose of adding zero motion is to adjust the trajectory of SGCMGs in the space of the gimbal angle so that the system can avoid the singularity nearby. When the system is far away from the internal singularity, e.g. $\min(\gamma_1, \gamma_2, \gamma_3, \gamma_4) > \pi/2$, it is not necessary to continue adding zero motion in order to save the system energy. Therefore, we further adjusted (36) to (38).

$$s_i = \begin{cases} 0 & if\ \gamma_i > \dfrac{\pi}{2} \\ \dfrac{|\pi/2 - \gamma_i + d| - |\pi/2 - \gamma_i - d|}{2d} & otherwise \end{cases} \tag{37}$$

$$\lambda = \max_i(s_i)\frac{\left\|\dot{\boldsymbol{\delta}}_\tau\right\|}{\max\left(\varsigma, \left|\hat{\mathbf{G}}\cdot\dot{\hat{\boldsymbol{\delta}}}_\tau\right|\right)}\hat{\mathbf{G}}\cdot\dot{\hat{\boldsymbol{\delta}}}_z \tag{38}$$

s_i is a switching function. If $\gamma_i > \pi/2$ (i=1,2,3,4), the SGCMG has been far away from the internal singularity, the zero motion does not need to be added. On this condition, we set $s_i = 0$ (i=1,2,3,4), λ is equal to 0. If $\pi/2 - d < \gamma_i < \pi/2$, the SGCMG is in the transitional region, then s_i takes a value of 0 to 1. If $\gamma_i < \pi/2 - d$, the SGCMG is in the singular escape region, then $s_i = 1$, the zero motion λ should be added.

E. SINGULARITY AVOIDANCE AND ESCAPE CONTROL STRATEGY

In order to deal with the potential singularity avoidance failure and enhance the robustness of the algorithm, the singularity escape steering law based on torque error is also needed as a supplementary strategy. The singularity escape control strategy is valuable only when the system has sufficient residual angular momentum, otherwise the system desaturation control strategy is adopted to reset the system. Based on the above analysis, we design a supplementary singularity escape steering law and integrate it with the aforementioned singularity avoidance steering law. The complete hybrid steering

law is given by (39).

$$\dot{\boldsymbol{\delta}} = \begin{cases} \dfrac{1}{h_0}\sum_{i=1}^{3}\hat{\mathbf{v}}_i\dfrac{1}{\sigma_i}\hat{\mathbf{u}}_i^T\boldsymbol{\tau}_d + \lambda\hat{\dot{\boldsymbol{\delta}}}_z \\ \quad \sigma_3 \geq \sigma_c,\ sse \geq \varepsilon \\ \dfrac{1}{h_0}\sum_{i=1}^{2}\hat{\mathbf{v}}_i\dfrac{1}{\sigma_i}\hat{\mathbf{u}}_i^T\boldsymbol{\tau}_d + \dfrac{1}{h_0}\hat{\mathbf{v}}_3\left(\dfrac{\sigma_3}{\sigma_c}\right)^2\dfrac{1}{\sigma_c}\hat{\mathbf{u}}_3^T\tau_d \\ +\left(\dfrac{\sigma_3}{\sigma_c}\right)^2\lambda\hat{\dot{\boldsymbol{\delta}}}_z + \left(1-\left(\dfrac{\sigma_3}{\sigma_c}\right)^2\right)\hat{\mathbf{G}} \\ \quad \sigma_3 < \sigma_c,\ and\ sse \geq \varepsilon_1 \\ \text{Desaturation Steering Strategy} \\ \quad sse < \varepsilon\ or \quad (\sigma_3 < \sigma_c, and\ sse < \varepsilon_1) \end{cases} \tag{39}$$

For (39), σ_c is a constant to distinguish singularity. If $\sigma_3 \geq \sigma_c$ and $sse > \varepsilon$, the system does not fall into singularity and the angular momentum of the system is not exhausted. The singularity avoidance steering law based on zero motion is applied. If $\sigma_3 < \sigma_c$ and $sse \geq \varepsilon_1$, the system has sufficient residual angular momentum. The singularity escape strategy is adopted to make the system escape from the singularity. If $\sigma_3 < \sigma_c$ and $sse < \varepsilon_1$, the system has insufficient residual angular momentum. It is of little significance to escape from singularity and the desaturation steering strategy should be adopted. If $sse < \varepsilon$, the angular momentum of the system has been exhausted, in this case the desaturation steering strategy should be adopted.

For $sse \geq \varepsilon_1$, the switching point between the singularity avoidance steering law and singularity escape steering law is at $\sigma_3 = \sigma_c$, and the values of $\dot{\boldsymbol{\delta}}$ on both sides of this switching point are continuous. If σ_3 continues to decrease and is less than σ_c, then the singularity escape steering law is activated. With the decrease of σ_3, the output torque of the system in $\hat{\mathbf{u}}_3$ becomes smaller and smaller, the added zero motion becomes smaller and smaller, and the component of $\hat{\mathbf{G}}$ in $\dot{\boldsymbol{\delta}}$ becomes larger and larger. The system can quickly escape from the singular state by using $\hat{\mathbf{G}}$.

V. SIMULATION COMPARISON AND DISCUSSION

The experimental parameters of SGCMGs with pyramid configuration are listed as follows. The amplitude of rotor angular momentum is $h_0 = 1Nms$, pyramid inclination is $\beta = 54.73°$, maximum gimbal angular velocity is $\dot{\delta}_{\max} = 180°/s$, simulation step is 0.01s and total simulation time is 10s. $\varepsilon = 0.2$, when $sse < \varepsilon$, the simulation is terminated. Desaturation control strategy is beyond the scope of discussion in this paper. The simulation is divided into two parts, singularity avoidance simulation and singularity escape simulation. For the simulation of singularity avoidance, the initial gimbal angle is $\boldsymbol{\delta} = \begin{bmatrix}0 & 0 & 0 & 0\end{bmatrix}$, and the following three typical torque are selected, $\boldsymbol{\tau}_{d1} = \begin{bmatrix}1 & 1 & 1\end{bmatrix}^T Nm$, $\boldsymbol{\tau}_{d2} = \begin{bmatrix}0.5 & 0.4 & 0.1\end{bmatrix}^T Nm$, and $\boldsymbol{\tau}_{d3} = \begin{bmatrix}-1 & 0 & 0\end{bmatrix}^T Nm$. There is no singularity in direction $\boldsymbol{\tau}_{d1}$, and there is singularity in direction $\boldsymbol{\tau}_{d2}$ and direction $\boldsymbol{\tau}_{d3}$, of which the singularity in direction $\boldsymbol{\tau}_{d3}$ is an internal elliptic singularity [4]. For the simulation of singularity escape, the initial gimbal angle is $\boldsymbol{\delta} = \begin{bmatrix}-\pi/2 & 0 & -\pi/2 & 0\end{bmatrix}$, this is an internal elliptical singularity [4], the desired torque is $\boldsymbol{\tau}_d = \begin{bmatrix}-1 & 0 & 0\end{bmatrix}^T Nm$. Under the action of $\boldsymbol{\tau}_d$, the system will move towards an internal impassable singular surface. On this condition, the system can only escape singularity by introducing a moment error.

The simulation results are shown in Fig. 7 to Fig. 31, each figure consists six subgraphs. From left to right, top to bottom, they are the output torque, norm of the total angular momentum, gimbal angular speed, gimbal angular position, effective residual angular momentum, and singularity measurement of the SGCMGs system, respectively. The ideal result of the simulation for singularity avoidance need to satisfy the following two points. First, the system can give relatively smooth angular velocity or position commands. Second, it should utilize all the angular momentum resources as quickly as possible and output the desired

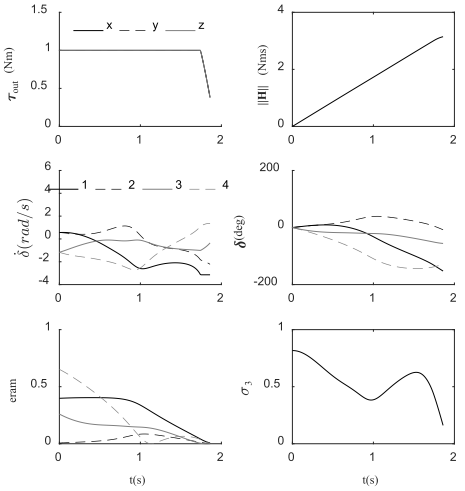

FIGURE 7. Simulation results of singularity avoidance of PI steering law for τ_{d1}.

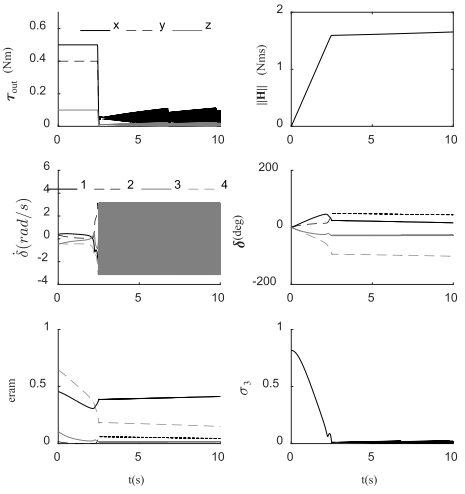

FIGURE 8. Simulation results of singularity avoidance of PI Steering Law for τ_{d2}.

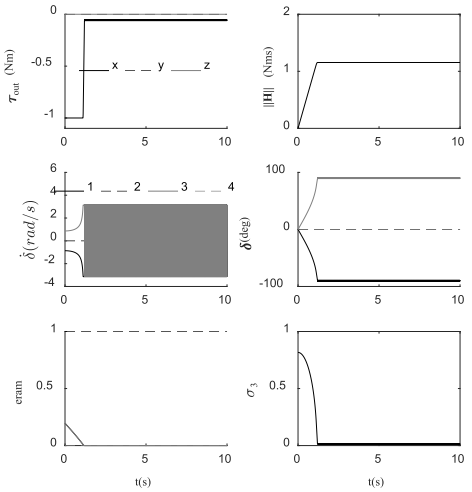

FIGURE 9. Simulation results of singularity avoidance of PI steering law for τ_{d3}.

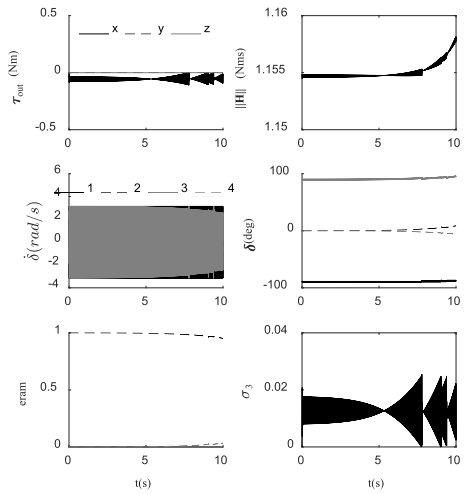

FIGURE 10. Simulation results of singularity escape of PI steering law for τ_d.

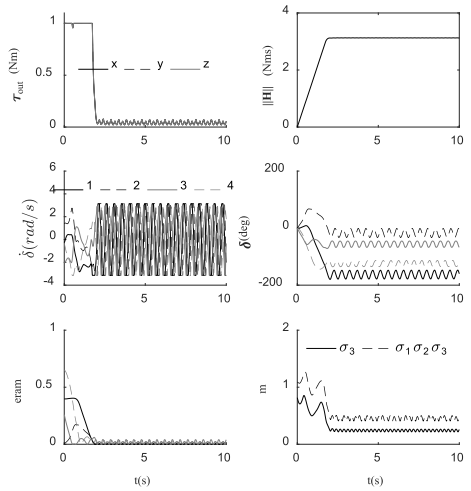

FIGURE 11. Simulation results of singularity avoidance of ND steering law for τ_{d1}.

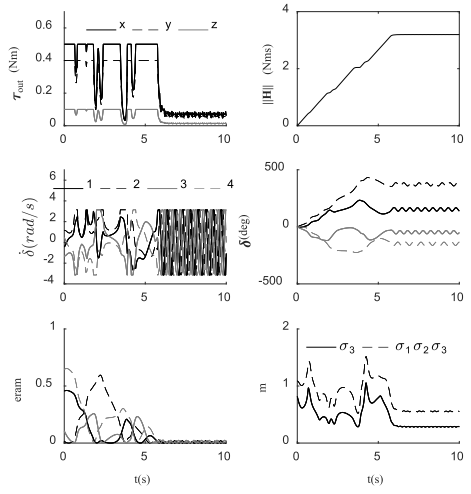

FIGURE 12. Simulation results of singularity avoidance of ND steering law for τ_{d2}.

torque accurately. The premise of accurate output torque of the system is that the system does not approach the singular state before it makes full use of all angular momentum resources (reaching saturated singularity), that is, the singular measure cannot approach zero before the end of the simulation. The simulation results of the ideal singularity escape steering law should have the following characteristics: first, the steering law can give smooth angular velocity instructions; second, the negative impact caused by the introduced torque error should be as small as possible; and finally, the system can escape from the singular state as soon as possible. Next, we will elaborate on the experimental results of five different steering laws.

A. PSEUDO-INVERSE STEERING LAW

In order to avoid the ill-conditioned solution of pseudo-inverse steering law, minor modifications are made to this law.

$$\dot{\boldsymbol{\delta}}_{PI} = \begin{cases} \dfrac{1}{h_0}\displaystyle\sum_{i=1}^{3}\hat{\mathbf{v}}_i\frac{1}{\sigma_i}\hat{\mathbf{u}}_i^T\boldsymbol{\tau}_d & \sigma_3 > 0.0001 \\ \dfrac{1}{h_0}\left(\displaystyle\sum_{i=1}^{2}\hat{\mathbf{v}}_i\frac{1}{\sigma_i}+\hat{\mathbf{v}}_3\frac{1}{0.0001}\right)\hat{\mathbf{u}}_i^T\boldsymbol{\tau}_d & otherwise \end{cases} \tag{40}$$

The simulation results are shown in Fig. 7 to Fig. 10. PI steering law does not possess the ability of singularity avoidance and escape. Fig. 7 shows that there is no singularity in the direction of $\boldsymbol{\tau}_{d1}$. At the end of the simulation, because the maximum gimbal angular velocity is limited, the magnitude of the command gimbal angular velocity is scaled down, so the magnitude of output torque decreases. Fig. 8 and Fig. 9 shows the system falls into internal singularities when it outputs $\boldsymbol{\tau}_{d2}$ and $\boldsymbol{\tau}_{d3}$. This verifies that

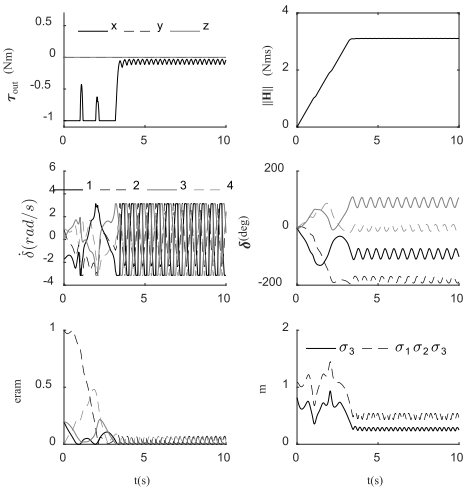

FIGURE 13. Simulation results of singularity avoidance of ND steering law for τ_{d3}.

there are the internal singularities in the direction of $\boldsymbol{\tau}_{d2}$ and $\boldsymbol{\tau}_{d3}$. Fig. 10 shows that PI steering law cannot make the system escape from the internal elliptical singularity at $\boldsymbol{\delta} = \begin{bmatrix} -\pi/2 & 0 & -\pi/2 & 0 \end{bmatrix}$.

B. NON-DIRECTIONAL NULL-MOTION ALGORITHM

The non-directional null-motion algorithm is a torque error free singularity avoidance steering law. We select this steering law for comparison because it is more successful in avoiding an elliptic-type internal singularity in the direction of $\boldsymbol{\tau}_{d3}$ [4]. The simulation results are shown in Fig.11 to Fig. 13.

As shown in Fig. 11 to Fig. 13, in the process of the system approaching saturation singularity, the gimbal angular velocity oscillates sharply, while the norm of the total angular momentum is almost unchanged. The reasons for this result are as follows. When the system is close to saturation singularity, the singular measurement value of the system is close to zero, then the steering law will add a very large zero motion. Because the maximum gimbal angular velocity is limited, the velocity components of the non-zero motion part will be greatly compressed, this results in almost no change in the amplitude of the total angular momentum of the system in the final stage. At the end of the simulation, the angular momentum resources of the system are almost exhausted, the singular measurement of the system is always greater than zero. The experimental result shows that the steering law has good singularity avoidance ability. However, both the angular velocity command and the torque fluctuate greatly.

C. OFF-DIAGONAL SINGULARITY-RUBUST STEERING LAW

The control parameters of ODSR steering law is shown in Table 1. According to the different settings of w_i parameters, we have done three different groups of experiments. The first group of experiments illustrates the singularity escape performance of the ODSR steering law, while the second and third groups illustrates the singularity avoidance and escape performance of the ODSR steering law.

TABLE 1. The control parameters of ODSR steering law.

	Value	Units
ε_0	0.1	— —
μ_0	0.01	— —
κ	10	— —
w	1	$rad\ /\ s$
ϕ_i	$\frac{\pi}{2}$	rad

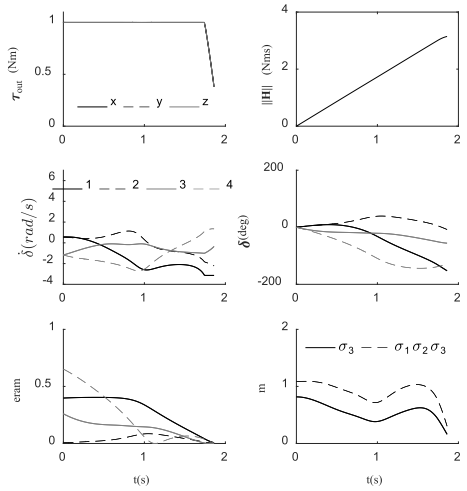

FIGURE 14. Simulation results of singularity avoidance of GSR steering law for τ_{d1}.

1) THE FIRST GROUP OF EXPERIMENTS

When $w_1 = w_2 = w_3 = w_4 = 1$, the ODSR steering law becomes the GSR steering law [11], [12]. The simulation results of the GSR steering law are shown from Fig. 14 to Fig. 17. When the system is far from singularity, the GSR steering law is equivalent to the PI steering law [11], which can be verified by comparing Fig. 7 with Fig. 14. This means that the GSR steering law is as easy to encounter singularity problems as the PI steering law. The PI steering law always falls into singularity, and the GSR steering law can escape singularity by introducing a torque error, and this is verified by comparing Fig. 8 with Fig. 15 and Fig. 9 with Fig. 16. However, the GSR steering law takes some time to get the system out of the singular state, and the angular velocity curve changes steeply, as shown in Fig. 16. Fig. 17 shows that the steering law can make the system escape from the singularity of internal ellipse.

2) THE SECOND AND THIRD GROUPS OF EXPERIMENTS

The corresponding parameters of the second group of experiments are as follows: $w_1 = 0.01$, $w_2 = w_3 = w_4 = 1$. The singularity avoidance simulation results are shown in Fig. 18 to Fig. 20. The corresponding parameters of the third group of experiments are as follows: $w_2 = 0.01$, $w_1 = w_3 = w_4 = 1$. As shown in Fig. 21 to Fig. 23, the

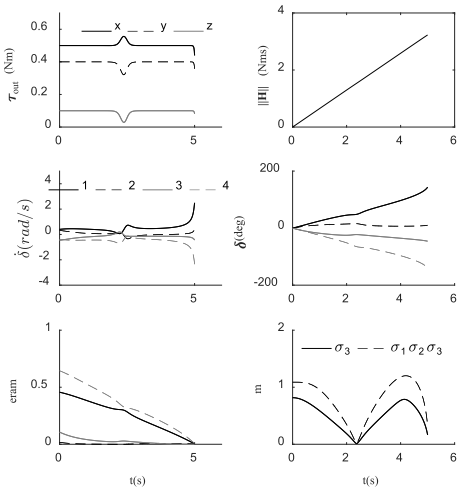

FIGURE 15. Simulation Results of singularity avoidance of GSR steering law for τ_{d2}.

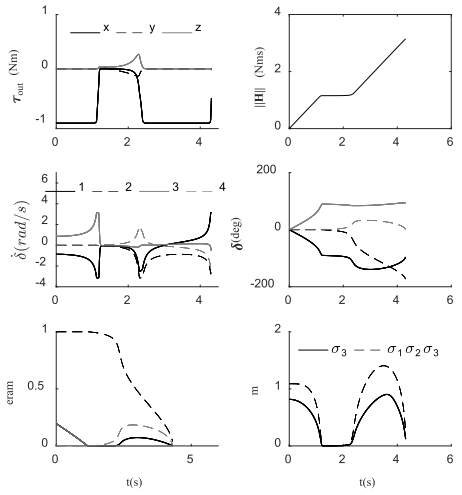

FIGURE 16. Simulation results of singularity avoidance of GSR steering law for τ_{d3}.

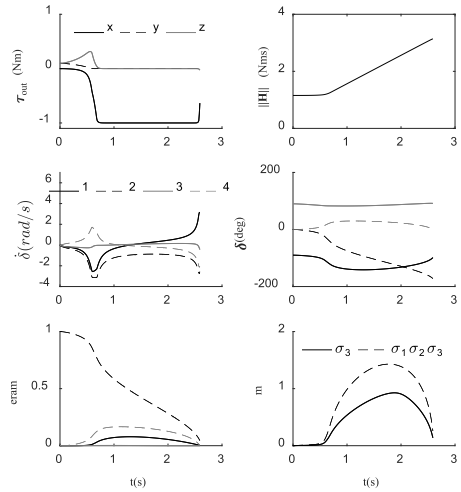

FIGURE 17. Simulation results of singularity escape of GSR steering law for τ_d.

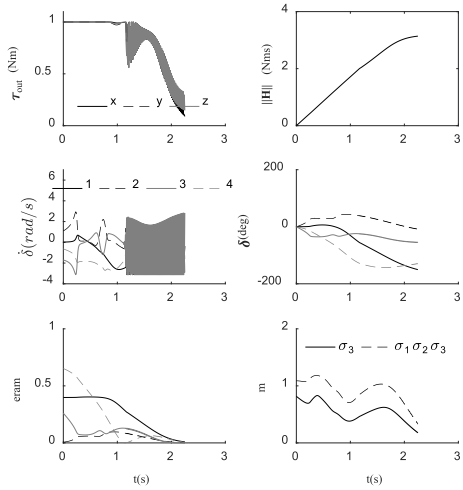

FIGURE 18. Simulation results of singularity avoidance of ODSR1 steering law for τ_{d1}.

experimental results are shown in Fig. 21 to Fig. 23. Some experimental results are analyzed as follows.

In the case of no singularity, corresponding to $\boldsymbol{\tau}_{d1}$, Compared with Fig. 18 and Fig. 21, the simulation results obtained in Fig. 14 are the best, which can be drawn from two aspects of the torque error and the angular velocity curve.

The comparison of the three figures (Fig. 15, Fig. 19 and Fig. 22) shows that Fig. 22 has the smallest torque error. Besides, under the parameters set in Fig. 22, the system does not encounter the singular state during the simulation. That is to say, in the direction of $\boldsymbol{\tau}_{d2}$, the third set of parameters has a better singularity avoidance capability.

Compared with Figs. 16 and 23, the simulation results obtained in Fig. 20 achieve the best performance. Under the parameters set in Fig. 20, the system has not encountered singularity problems. This verifies that the second set of parameters has better singularity avoidance capability in direction of $\boldsymbol{\tau}_{d3}$. In addition, the angular velocity curves of the three groups change drastically.

From the above analysis, it can be concluded that the ODSR steering law is a hybrid steering law with singularity avoidance and escape capability. However, its singular avoidance ability depends heavily on the design of parameters. The torque error is often introduced in the process of singularity avoidance or escape. In addition, velocity curve generated by ODSR often has steep changes.

D. DIRECTIONAL SINGULARITY ESCAPE AND AVOIDANCE STEERING LAW

We set the same experimental parameters as Reference [23], except for $\tau_{\max}$. We modify $\tau_{\max}$ from 10 to 2Nm according to the simulation conditions in this paper, as shown in Table 2. The simulation results are shown from Fig. 24 to Fig. 27.

The simulation results from Fig. 25 to Fig. 27 show that the gimbal angular velocity curve is smooth and the singular measurement never equals to zero. However, torque error exists

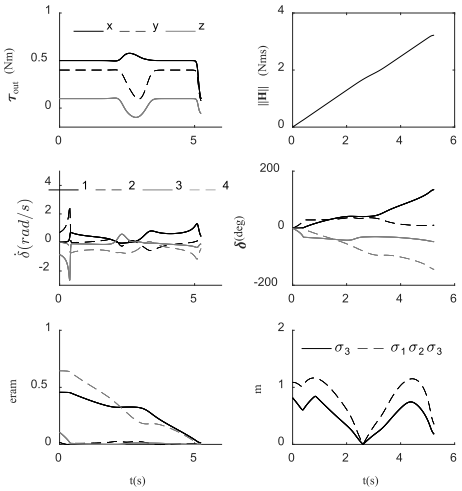

FIGURE 19. Simulation results of singularity avoidance of ODSR1 steering law for τ_{d2}.

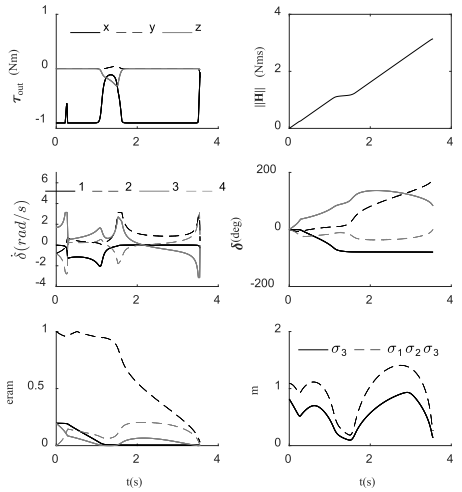

FIGURE 20. Simulation results of singularity avoidance of ODSR1 steering law for τ_{d3}.

TABLE 2. The experimental parameters of DSEA steering law.

	Value	Units
σ_{acp}	0.75	— —
$\sigma_{\min}$		
η	10	— —
d_0	3	*rad / s*
$\tau_{\min}$	0.001	*Nm*
$\tau_{\max}$	2	*Nm*
ξ	0.5	— —

in all three kinds of torques. Fig. 27 shows that the DSEA steering law can make the system out of the internal elliptical singularity. As theoretically analyzed in the previous chapter, DSEA steering law sacrifices the precision of the output torque for the singularity avoidance performance.

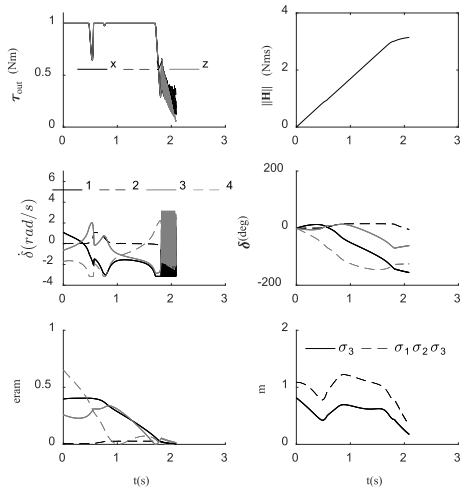

FIGURE 21. Simulation results of singularity avoidance of ODSR2 steering law for τ_{d1}.

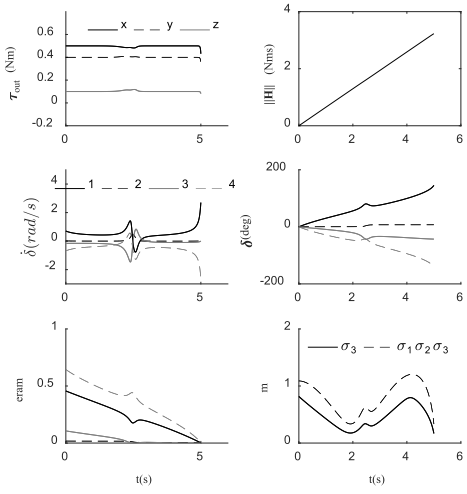

FIGURE 22. Simulation results of singularity avoidance of ODSR1 steering law for τ_{d2}.

TABLE 3. The control parameters of the proposed VCBSAE steering law.

Parameter	Value
ς	0.1
ξ	1
d	0.1
ε_1	0.8
σ_c	0.1

E. VECTOR-CONTROL BASED SINGULARITY AVOIDANCE AND ESCAPE STEERING LAW

The control parameters of the proposed VCBSAE steering law are given in Table 3. The simulation results are shown from Fig. 28 to Fig. 31.

The results of Figs. 28 and 29 are very ideal, with no torque error, no singularity, and very flat angular velocity command. In Fig. 30, due to the limitation of the maximum

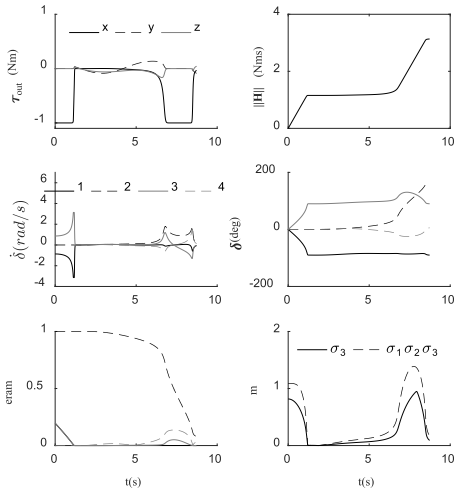

FIGURE 23. Simulation results of singularity avoidance of ODSR2 steering law for τ_{d3}.

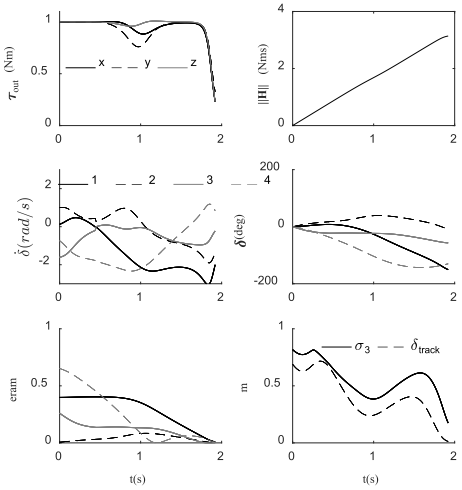

FIGURE 24. Simulation results of singularity avoidance of DSEA steering Law for τ_{d1}.

gimbal angular velocity, the amplitude of the speed command signal is compressed. Although the amplitude of the output torque is compressed in the same proportion, the direction of the output torque can remain unchanged. In addition, when the command torques are $\boldsymbol{\tau}_{d2}$ and $\boldsymbol{\tau}_{d3}$, the system does not encounter singularities and the angular velocity curves are relatively flat. Fig. 31 shows the VCBSAE steering law can make the system escape from the internal elliptical singularity. The experimental results show that the proposed steering law has strong singularity avoidance and escape ability.

F. SUMMARY

1) SINGULARITY AVOIDANCE

The experimental comparison of singular avoidance is summarized in Tables 4 to 6. For different command torques, we summarize the performance of the different steering laws from five aspects: torque error, gimbal velocity, singular measurement, total time of simulation and momentum reserve. If the direction of the output torque is different from that of the command moment in the simulation, that is, there is a torque error, then fill in Y in the corresponding cell, otherwise fill in N. If the gimbal angular velocity changes dramatically, then fill in Y in the corresponding cell, otherwise fill in N. If the minimum value of singular measure is zero, then Y is filled in the corresponding cell, otherwise N is filled.

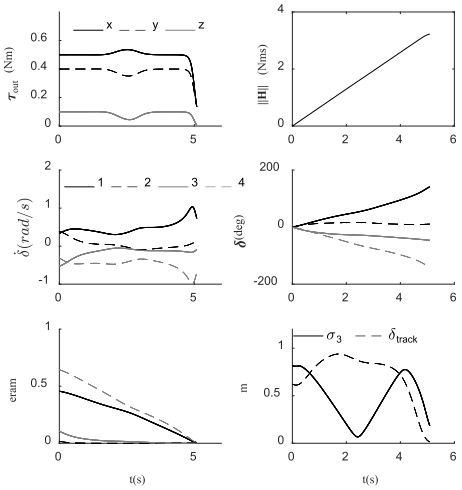

FIGURE 25. Simulation results of singularity avoidance of DSEA steering law for τ_{d2}.

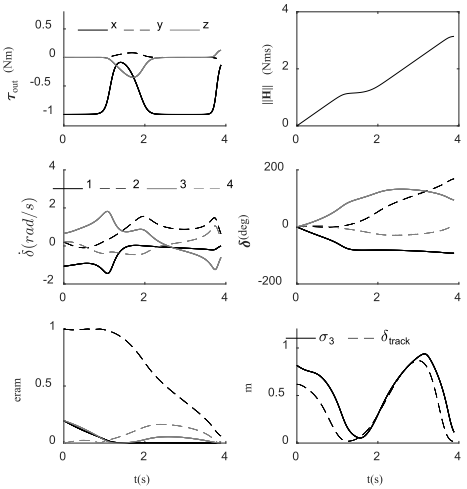

FIGURE 26. Simulation results of singularity avoidance of DSEA steering law for τ_{d3}.

TABLE 4. The performance of different steering laws in the direction of τ_{d1}.

$\boldsymbol{\tau}_{d1}$	Torque error	Gimbal velocity	Singular measure	Total time(s)	Momentum reserve(Nms)
PI	N	N	N	1.86	0.02214
ND	N	Y	N	10	0.03775
GSR	N	N	N	1.86	0.02634
ODSR1	Y	Y	N	2.25	0.03154
ODSR2	Y	Y	N	2.09	0.02839
DSEA	Y	N	N	1.92	0.03289
VCBSAE	N	N	N	1.86	0.02563

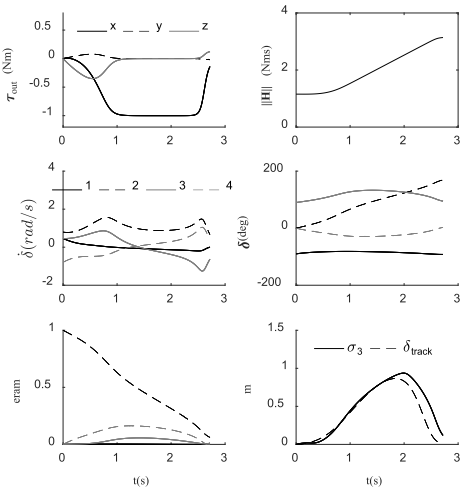

FIGURE 27. Simulation results of singularity escape of DSEA steering law for τ_d.

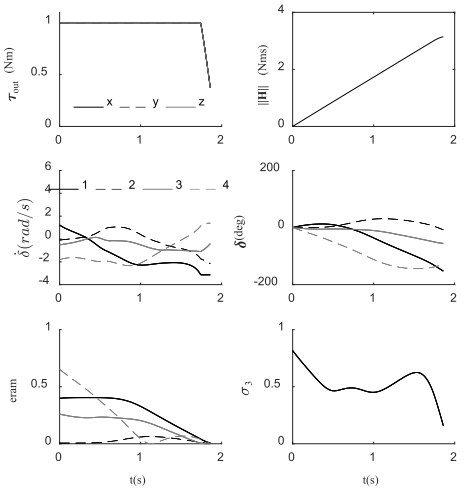

FIGURE 28. Simulation results of singularity avoidance of VCBSAE steering law for τ_{d1}.

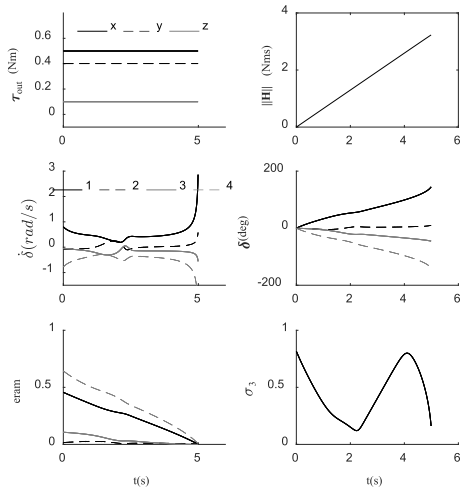

FIGURE 29. Simulation results of singularity avoidance of VCBSAE steering law for τ_{d2}.

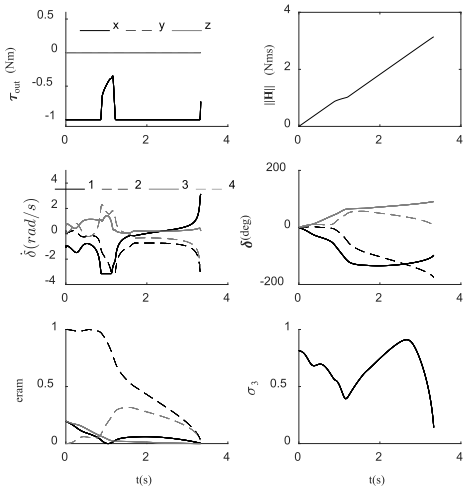

FIGURE 30. Simulation results of singularity avoidance of VCBSAE steering law for τ_{d3}.

From Table 4 to Table 6, it can be concluded that for different desired torques, only the proposed steering law can simultaneously have torque error free, relatively stable angular velocity and strong singularity avoidance ability. The time consumed for the VCBSAE steering law is the shortest except for PI steering. In addition, in all simulations lasting less than 10 seconds, the angular momentum of the system is almost exhausted and the system does not fall into saturation singularity. This proves the validity of *sse*.

TABLE 5. The performance of different steering laws in the direction of τ_{d2}.

τ_{d2}	Torque error	Gimbal velocity	Singular measure	Total time(s)	Momentum reserve(Nms)
PI	N	Y	Y	10	1.453
ND	N	Y	N	10	0.04893
GSR	Y	N	Y	5	0.02646
ODSR1	Y	Y	Y	5.24	0.03313
ODSR2	Y	N	N	5	0.02738
DSEA	Y	N	N	5.09	0.03004
VCBSAE	N	N	N	4.99	0.02588

2) SINGULARITY ESCAPE

We measure the singular escape performance of the steering law from the following aspects: total time, impulse moment deviation introduced by X and Y direction error moments, and total impulse moment deviation. Table 7 shows the simulation results of singularity escape for GSR, DSEA and VCBSAE steering laws. The GSR steering law has the shortest total time and the smallest total impulse moment deviation, it achieves the best escape performance, followed by our algorithm, and finally DSEA algorithm. This verifies that the steering law designed in this paper can make the system escape from singularity, and its performance is between GSR and DSEA steering laws.

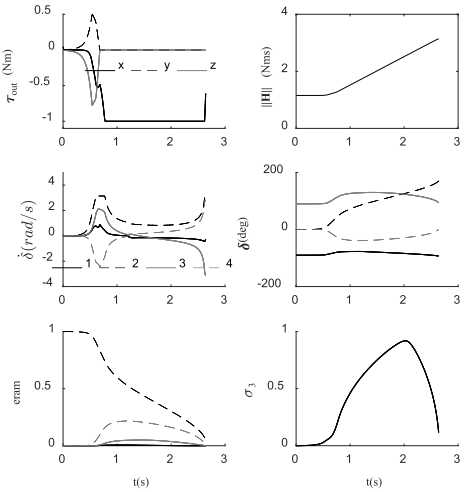

FIGURE 31. Simulation results of singularity escape of VCBSAE steering law for τ_d.

TABLE 6. The avoidance performance of different steering laws in the direction of τ_{d3}.

τ_{d3}	Torque error	Gimbal velocity	Singular measure	Total time(s)	Momentum reserve(Nms)
PI	N	Y	Y	10	2
ND	N	Y	N	10	0.04701
GSR	Y	Y	Y	4.31	0.01065
ODSR1	Y	Y	N	3.55	0.01724
ODSR2	Y	Y	Y	8.73	0.02129
DSEA	Y	N	N	3.86	0.01628
VCBSAE	N	N	N	3.33	0.01236

TABLE 7. The escape performance of different steering laws.

$\tau_d=[-1 \quad 0 \quad 0]^T$ (Nm)	Total time(s)	$\int_0^t \tau_{d_y} dt$ (Nms)	$\int_0^t \tau_{d_z} dt$ (Nms)	τ_e (Nms)
GSR	2.59	0.03779	0.1243	0.1299
DSEA	2.72	0.0441	-0.2005	0.2053
VCBSAE	2.64	0.09281	-0.1479	0.1746

VI. CONCLUSION

By comparing with PI steering law, ND steering law, GSR steering law, ODSR steering law and DSEA steering law, we verify that the proposed steering law is the only one possess the following four advantages at the same time.

a. It can reach the angular momentum boundary almost as fast as pseudo-inverse steering law in the absence of singularity.

b. It has the strongest singularity avoidance ability.

c. On the premise of introducing moment error, it can make the system quickly escape from the internal elliptic singularity.

d. The angular velocity command given by the proposed steering law will not produce severe oscillation.

REFERENCES

[1] J. Crenshaw, "2-SPEED, a single-gimbal control moment gyro attitude control system," *Proc. AIAA*, Aug. 1973, pp. 73–895.
[2] G. Margulies and J. N. Aubrun, "Geometric theory of single-gimbal control moment gyro systems," *J. Astron. Sci.*, vol. 26, no. 2, pp. 159–191, 1978.
[3] D. E. Cornick, "Singularity avoidance control laws for single gimbal control moment gyros," in *Proc. Guid. Control Conf.*, vol. 1698, 1979, pp. 255–267.
[4] N. Bedrossian, J. A. Paradiso, E. Bergmann, and D. Rowell, "Steering law design for redundant single-gimbal control moment gyroscopes," *J. Guid. Control Dyn.*, vol. 13, no. 6, pp. 1083–1089, 1990.
[5] H. Leeghim, H. Bang, and J.-O. Park, "Singularity avoidance of control moment gyros by one-step ahead singularity index," *Acta Astronautica*, vol. 64, nos. 9–10, pp. 935–948, 2009.
[6] C. Li, Y. Guo, and G. Ma, "Singularity analysis and steering law design for single-gimbal control moment gyroscopes," *J. Astronautics*, vol. 31, no. 10, pp. 2346–2353, 2010.
[7] S. R. Vadali, H. S. Oh, and S. R. Walker, "Preferred gimbal angles for single gimbal control moment gyros," *AIAA J. Guid. Control Dyn.*, vol. 13, no. 6, pp. 1090–1095, 1990.
[8] J. A. Paradiso, "Global steering of single gimballed control moment gyroscopes using a directed search," *AIAA J. Guid. Control Dyn.*, vol. 15, no. 5, pp. 1236–1244, 1992.
[9] W. Zhang, Y. Zhang, and W. Li, "Path Planning for Rapid Large-Angle Maneuver of Satellites Based on the Gauss Pseudo spectral Method," *Math. Problems Eng.*, vol. 2016, Feb. 2016, Art. no. 1081267.
[10] Z. Sun and S. Ding, "SGCMG non-singularity steering based on adaptive Gauss pseudospectral method," in *Proc. IEEE ICCSS*, Oct. 2014, pp. 96–101.
[11] B. Wie, C. Heiberg, and D. Bailey, "Singularity robust steering logic for redundant single-gimbal control moment gyros," *J. Guid. Control Dyn.*, vol. 24, no. 5, pp. 865–872, Sep./Oct. 2001.
[12] B. Wie, "Singularity escape/avoidance steering logic for control moment gyro systems," *AIAA J. Guid. Control Dyn.*, vol. 28, no. 5, pp. 948–956, Sep./Oct. 2005.
[13] K. A. Ford and C. D. Hall, "Singular direction avoidance steering for control-moment gyros," *J. Guid., Control, Dyn.*, vol. 23, no. 4, pp. 648–656, 2000.
[14] T. Meng and S. Matunaga, "Modified singular-direction avoidance steering for control moment gyros," *AIAA J. Guid. Control Dyn.*, vol. 34, no. 6, pp. 1915–1920, 2011.
[15] Y. Guo, H. Cui, G. Ma, and C. Li, "Singular direction escape steering law for control moment gyros," *J Aerosp. Eng*, vol. 30, no. 5, 2017.
[16] K. Takada, H. Kojima, and N. Matsuda, "Control moment gyro singularity-avoidance steering control based on singular-surface cost function," *AIAA J. Guid. Control Dyn.*, vol. 33, no. 5, pp. 1442–1450, Sep./Oct. 2010.
[17] K. Yamada and I. Jikuya, "Directional passability and quadratic steering logic for pyramid-type single gimbal Control Moment Gyros," *Acta Astronautica*, vol. 102, pp. 103–123, Sep./Oct. 2014.
[18] Y. Geng, Z. Hou, and J. Guo, "Rapid singularity-escape steering strategy for single-gimbal control moment gyroscopes," *AIAA J. Guid. Control Dyn.*, vol. 40, no. 12, pp. 3199–3210, 2017.
[19] J. Guo, B. Wu, Y. Geng, X. Kong, and Z. Hou, "Rapid SGCMGs singularity-escape steering law in gimbal angle space," *IEEE Trans. Ind. Electron.*, vol. 54, no. 5, pp. 2509–2525, Oct. 2018.
[20] O. Tekinalp and E. Yavuzoglu, "A new steering law for redundant control moment gyroscope clusters," *Aerosp Sci Technol*, vol. 9, no. 7, pp. 626–634, 2005.
[21] L. Wang, Y. Guo, L. Wu, and Q. Cheng, "Improved optimal steering law for SGCMG and adaptive attitude control of flexible spacecraft," *J. Syst. Eng. Electron.*, vol. 26, no. 6, pp. 1268–1276, Dec. 2015.
[22] F. A. Leve and N. Fitz-Coy, "Hybrid steering logic for single-gimbal control moment gyroscopes," *AIAA J. Guid. Control Dyn.*, vol. 33, no. 4, pp. 1202–1212, 2010.
[23] L. Valk, A. Berry, and H. Vallery, "Directional singularity escape and avoidance for single-gimbal control moment gyroscopes," *AIAA J. Guid. Control Dyn.*, vol. 41, no. 5, pp. 1107–1195, 2018.
[24] H. Kurokawa, "Survey of theory and steering laws of single-gimbal control moment gyros," *J. Guid. Control Dyn.*, vol. 30, no. 5, pp. 1331–1340, 2007.
[25] F. A. Leve, "Evaluation of steering algorithm optimality for single-gimbal control moment gyroscopes," *IEEE Trans. Control Syst. Technol.*, vol. 22, no. 3, pp. 1130–1134, May 2014.

[26] F. A. Leve, A. L. Frederick, B. J. Hamilton, and M. A. Peck, "Singularities of control moment gyroscopes," in *Spacecraft Momentum Control Systems*. Switzerland: Springer, 2015, pp. 95–131.
[27] Z. L. Hou, Y. H. Geng, B. L. Wu, and S. M. Huang, "Spacecraft angular velocity trajectory planning for SGCMG singularity avoidance," *Acta J. Astronaut*, vol. 151, pp. 284–295, 2018.
[28] J. Zhang, K. Ma, G. Meng, and S. Tian, "Spacecraft maneuvers via singularity-avoidance of control moment gyros based on dual-mode model predictive control," *IEEE Trans. Aerosp. Electron. Syst.*, vol. 51, no. 4, pp. 2546–2559, Oct. 2015.
[29] K. Yamada, T. Asai, and I. Jikuya, "Inverse kinematics in pyramid type single-gimbal control moment gyro system," *AIAA J. Guid. Control Dyn.*, vol. 39, no. 8, pp. 1897–1907, 2016.
[30] T. Kanzawa, M. Haruki, and K. Yamanaka, "Steering law of control moment gyroscopes for agile attitude maneuvers," *AIAA J. Guid. Control Dyn.*, vol. 39, no. 4, pp. 952–962, 2016.
[31] J. Guo, Y. Geng, B. Wu, and X. Kong, "Vibration suppression of flexible spacecraft during attitude maneuver using CMGs," *Aerosp. Sci. Technol.*, vol. 72, pp. 183–192, Jan. 2018.

NING MAO was born in Heilongjiang, China, in 1993. He received the B.E. degree from the Harbin Institute of Technology, in 2015. He is currently pursuing the Ph.D. degree with the University of Chinese Academy of Sciences and the Changchun Institute of Optics, Fine Mechanics and Physics, Chinese Academy of Sciences, China.

His research interests include satellite attitude and control, modeling, parameter identification, as well as electric machine drives and control.

TAO ZHANG was born in Jilin, China, in 1964. He received the B.E. degree from Zhejiang University, in 1987.

From 1987 to 2008, he has served as a Deputy Researcher of the Photoelectric Engineering Department, the Deputy Director of the Scientific Research Department, the Director of the Optical Engineering Center, the Deputy Director of the Photoelectric Engineering Department, a Researcher, as well as the Director of the Aviation Surveillance Department and the General Manager of the Opp Photoelectric Technology Company, Ltd., Changchun Institute of Optics, Fine Mechanics and Physics, Chinese Academy of Sciences. From 2008 to 2012, he has served as the Deputy Group Leader of the Preparation Team, Suzhou Institute of Biomedical Engineering Technology (preparatory), Chinese Academy of Sciences, the Director of the Medical Image Technology Research Department (concurrently: Assistant Director of Changchun Institute of Optics, Fine Mechanics and Physics, Chinese Academy of Sciences, in 2010), and the Vice President of the Changchun Optical Machinery Institute, since 2012. His research interests include detection and imaging technology and stability control technology.

Dr. Zhang has won two second-class prizes for scientific and technological progress of the Chinese Academy of Sciences, one third-class prize for scientific and technological progress of the Chinese Academy of Sciences, as well as one National Invention Patent Award, and enjoys the government subsidy of the State Council.

KAI XU was born in Heilongjiang, China, in 1982. He received the B.E. degree from Jilin University, in 2004, and the M.S. and Ph.D. degrees from the Changchun Institute of Optics, Fine Mechanics and Physics, Chinese Academy of Sciences, China, in 2009.

From 2009 to 2015, he was a Deputy Researcher of the Spaceborne Technology Research Laboratory, Changchun Institute of Optics, Fine Mechanics and Physics, Chinese Academy of Sciences. From 2015 to 2018, he was the Director of the Research Laboratory of Attitude and Orbit Control Technology, Chang Guang Satellite Technology Co., Ltd. Since 2018, he has been with the Minister of Scientific Research Quality, Chang Guang Satellite Technology Company, Ltd. His research interests include satellite dynamics modeling, attitude and orbit control, and so on.

MAO-SHENG CHEN was born in Jiangsu, China, in 1985. He received the B.S. degree from the Nanjing University of Science and Technology, in 2007, and the M.S. and Ph.D. degrees from the Changchun Institute of Optics, Fine Mechanics and Physics, Chinese Academy of Sciences, China, in 2012.

From 2012 to 2015, he was a Deputy Researcher with the Spaceborne Technology Research Laboratory, Changchun Institute of Optics, Fine Mechanics and Physics, Chinese Academy of Sciences. Since 2015, he has been the Director of the Integrated Electronics Research, Chang Guang Satellite Technology Company, Ltd. His research interests include embedded system design and motor servo control.

CHAO DONG was born in Jilin, China, in 1992. She received the B.E. degree from Jilin University, in 2015. She is currently pursuing the Ph.D. degree with the University of Chinese Academy of Sciences and the Changchun Institute of Optics, Fine Mechanics and Physics, Chinese Academy of Sciences, China.

Her research interests include satellite earth observation and satellite data analysis.